A composite analytical model to predict the thermal performance of borehole ground heat exchangers within stratified ground

Wu Gao [a, b, c, d] *, **Meysam Qadrdan** [d]

[a] Institute of Geotechnical Engineering, Zhejiang University, Hangzhou, 310058, China

[b] Center for Hypergravity Experimental and Interdisciplinary Research, Zhejiang University, Hangzhou, 310058, China

[c] MOE Key Laboratory of Soft Soils and Geoenvironmental Engineering, Zhejiang University, Hangzhou, 310058, China

[d] School of Engineering, Cardiff University, The Queen's Building, The Parade, Cardiff, CF24 3AA, United Kingdom

* Corresponding author:

Wu Gao

gaowu@zju.edu.cn, gaowu_ed@163.com

+86-18858155495

Abstract:

The thermal performance of borehole ground heat exchangers is of significance to the efficacy of the ground source heat supply systems. This paper presents a new composite analytical model to evaluate the thermal performance of borehole ground heat exchangers within stratified ground. The model integrates critical factors influencing heat transfer, encompassing ground stratification, thermal interactions among boreholes, variability of heat flux along borehole depth, and flexible layouts of boreholes. It enables efficient computation of thermal data pertinent to heat transfer both inside and outside the boreholes during operation. Implemented in the TRNSYS platform, the model offers versatile applicability to ground-source heat pump systems, borehole thermal energy storage, and district heating and cooling networks. Model validations were carried out through four distinct experiments, covering varied borehole quantities and ground conditions, to substantiate its accuracy. Employing this model, a case study further investigated the thermal performance of a borehole field with 16 boreholes in a three-layer ground (comprising backfill soil, clay, and fine sand) extending to a depth of 63 m. Over a 60-day warm water injection period at 30°C, the effects of borehole layout and ground stratification on the thermal performance of individual and collective boreholes were analysed. Key findings in this analysis include: (1) Across the square, L-shape, and linear layouts, the impact of layout on the thermal performance of borehole fields diminishes as the spacing increases from 1 m, 2 m, and 3m, becoming negligible at 4-m spacing, and the positions of the most and least affected boreholes by thermal interferences vary by layout; (2) Designing a GSHP system in stratified ground using a homogenous ground model with equivalent thermal properties would overestimate the heat injection performance of the borehole field and lead to undersizing of the borehole ground heat exchangers; and (3) ground stratification should be considered when estimating the thermal performance of a borehole field, particularly when the boreholes are sparsely arranged, e.g., with spacing of 3 m or more.

Keywords: Borehole ground heat exchanger, Thermal performance, Analytical model, Ground stratification, Borehole layout, Ground source heat supply system

Nomenclature

Symbols or terms	Physical meaning	Unit
r_b	Borehole radius	m
d	Borehole spacing	m
L	Borehole length	m
z	Depth of the ground layer	m
Δz	Length of the borehole section	m
r_{po}	Outer radius of the pipe	m
r_{pi}	Inner radius of the pipe	m
x_c	Shank spacing	m
r_g	Radial location of the grout node	m
r_{eq}	Equivalent radius	m
x	Coordinate of the borehole location along the *x*-axis	m
y	Coordinate of the borehole location along the *y*-axis	m
h	Vertical distance from the heat source to the ground surface	m
S	Distance between sections along the energy path	m
S'	Distance between sections along the imaginary energy path	m
ρ	Density of the ground layer	kg/m^3
α	Thermal diffusivity of the ground layer	m^2/s
λ	Thermal conductivity of the ground layer	W/m/K
c_p	Specific heat capacity of the ground layer	J/kg/K
ρ_{comp}	Composite density of the ground layer	kg/m^3
α_{comp}	Composite thermal diffusivity of the ground layer	m^2/s
λ_{comp}	Composite thermal conductivity of the ground layer	W/m/K
c_{pcomp}	Composite specific heat capacity of the ground layer	J/kg/K
ρ'_{comp}	Composite density of the imaginary ground layer	kg/m^3
α'_{comp}	Composite thermal diffusivity of the imaginary ground layer	m^2/s
λ'_{comp}	Composite thermal conductivity of the imaginary ground layer	W/m/K
c'_{pcomp}	Composite specific heat capacity of the imaginary ground layer	J/kg/K
ρ_g	Density of the grout material	kg/m^3
α_g	Thermal diffusivity of the grout material	m^2/s
λ_g	Thermal conductivity of the grout material	W/m/K
c_{pg}	Specific heat capacity of the grout material	J/kg/K
ρ_f	Density of the fluid	kg/m^3
α_f	Thermal diffusivity of the fluid	m^2/s
λ_f	Thermal conductivity of the fluid	W/m/K
c_{pf}	Specific heat capacity of the fluid	J/kg/K
m_f	Mass flow rate of the fluid	kg/s
u_f	Flow velocity of the fluid	m/s
μ_f	Dynamic viscosity of the fluid	kg/m/s
q	Heat flux	W/m
N_u	Nusselt number	-
P_r	Prandtl number	-
R_e	Reynolds number	-

Δt	Time step	s
T_{f1}	Downward fluid temperature	K or ℃
T_{f2}	Upward fluid temperature	K or ℃
T_b	Borehole wall temperature	K or ℃
ΔT_b	Borehole wall temperature increment	K or ℃
T_g	Temperature of the grout material	K or ℃
T_{Ground}	Ground temperature	K or ℃
T_{in}	Inlet fluid temperature	K or ℃
T_{out}	Outlet fluid temperature	K or ℃
C_f	Thermal capacitance of the fluid	J/m/K
C_g	Thermal capacitance of the grout material	J/m/K
R_{gb}	Thermal resistance between the grout material and borehole wall	K·m/W
R_{fg}	Thermal resistance between the fluid and grout material	K·m/W
R_{ff}	Thermal resistance between two legs of the pipe in a borehole	K·m/W
R_a	Interference thermal resistance	K·m/W
R_b	Equivalent thermal resistance of the borehole	K·m/W
R_g	Thermal resistance of the grout material	K·m/W
$R_{conduction}$	Conductive resistance of the pipe	K·m/W
$R_{convection}$	Convective resistance of the fluid	K·m/W
P	Heat injection rate	kW
h_{heat}	Convective heat transfer coefficient	W/m^2/K
λ_1	Dimensionless parameter	-
λ_2	Dimensionless parameter	-
λ_3	Dimensionless parameter	-
σ	Dimensionless parameter	-
M	Total number of sublayers	-
m	Number of the ground layer	
n	Number of the ground layer or number of the sample data points	-
N	Total number of boreholes	-
i	Identifier of the borehole	-
j	Identifier of the borehole	-
u	Identifier of the borehole section	-
v	Identifier of the borehole section	-
w	Identifier of the borehole section	-
l	Number of layers in the energy path	-
k	Identifier of layers in the energy path or time step index	-
b	Borehole well	-
g	Grout material	-
f	Fluid or friction factor	-
SR	Simulated results	-
MR	Measured results	-

1. Introduction

Ground-source heat pump (GSHP) systems, which utilize the ground as a heat source or sink, offer an energy-efficient approach of using geothermal energy for heating and cooling while reducing greenhouse gas emissions from the currently prevalent fossil-based heating systems (Minaei and Maerefat, 2017a; Gawecka et al., 2020; Alaie et al., 2021). Central to GSHP systems are ground heat exchangers, responsible for transferring heat to or from the ground. Vertical boreholes, a widely used type of ground heat exchanger, are known for their high thermal efficiency, minimal site area requirements, and limited influence from surface temperature fluctuations (Molina-Giraldo et al., 2011; Li and Lai, 2012). Borehole thermal energy storage also shows high efficiency in seasonal thermal storage, with promising application in district heating and cooling networks (Gao et al., 2023a; Ricks et al., 2024). Nonetheless, boreholes face high drilling costs, and their thermal performance is critical to the overall efficiency of the system. Therefore, it is imperative to comprehensively evaluate the thermal performance of boreholes during the design phase prior to their implementation.

Multiple factors influence the thermal performance of borehole ground heat exchangers, which can be broadly categorized as follows: i) site conditions, including ground layer composition, geothermal gradient of the ground, and groundwater flow, which are often encountered along the depth of boreholes (Hu, 2017; Li et al., 2020; Zhou et al., 2021; Bao et al., 2023; Guo et al., 2023); ii) ground characteristics, including soil thermal conductivity, density, and specific heat capacity, which exhibit significant variability across different soils (Abdelaziz et al., 2014; Li et al., 2018; Li et al., 2019; Li et al., 2023; Jin et al., 2020); iii) system configurations and design, encompassing parameters such as borehole quantity, depth, diameter, spacing, connection type, borehole interactions, and the grouting materials, which are tailored to specific geological conditions and engineering projects (Beier et al., 2011; Kurevija et al., 2012; Al-Khoury and Focaccia, 2016; Law and Dworkin, 2016; Li et al., 2019; Gultekin et al., 2019; Alaie et al., 2021; Cassina et al., 2022; Bandeira Neto et al., 2023); and iv) operational conditions, including thermal load, operational continuity, and flow rate, etc., which are intricately linked to the specific application scenarios (Shen et al., 2023; Li et al., 2019; Li et al., 2020; Hefni et al., 2022).

Given the importance and complexity of borehole thermal performance, various numerical models have been developed, predominantly employing the finite difference method (Lee and Lam, 2008; Lee, 2011; Lee and Lam, 2012; Zong et al., 2021), the finite element method (Ozudogru et al., 2014; Law and Dworkin, 2016; Gawecka et al., 2020; Gao et al., 2023b), and the finite volume method (Kurnia et al.,

2021; Pokhrel et al., 2022). For example, Lee and Lam (2008) used three-dimensional (3D) implicit finite difference method with rectangular coordinate system to simulate the thermal response of boreholes in homogenous ground, later extending this model to multi-layered ground conditions (Lee and Lam, 2012). Law and Dworkin (2016) utilized the commercial software COMSOL Multiphysics to create a 3D finite element model simulating multiple boreholes in GSHP operation, while Gao et al. (2023b) developed a coupled thermal–hydraulic model for unsaturated soils within the finite element platform COMPASS, comparing the thermal performance of horizontal and vertical ground heat exchangers in GSHP systems. Additionally, Kurnia et al. (2021) adopted the finite volume software ANSYS Fluent to investigate the temperature profiles of abandoned oil wells as geothermal boreholes, and Pokhrel et al. (2022) developed a 3D coupled fluid flow and heat transfer model using a finite volume approach for geothermal energy production of vertical coaxial heat exchanger. These models are adept at accounting for diverse heat transfer mechanisms and influential factors within both the borehole and the surrounding ground, thereby producing a high degree of accuracy (Zhang et al., 2022). However, numerical modelling can be computationally intensive, making it unsuitable for long-time simulations (e.g., 20 years) in projects involving large-scale borehole fields (Yang et al., 2014; Al-Khoury and Focaccia, 2016; Hu et al., 2017).

Apart from numerical modelling, analytical models have emerged as valuable tools for studying the thermal performance of boreholes, offering simplicity and inherently low computational costs (Alaie et al., 2021; Zhang et al., 2022; Guo et al., 2023). These models have found utility both in theoretical investigations and practical applications. Based on the features and functions, existing analytical models for boreholes in literature can be organized into the following three categories.

Line source models represent a classic category of analytical models to analyse heat transfer phenomena external to boreholes, focusing on thermal responses like borehole wall temperature. These models operate under the assumption that the borehole behaves as a line source, owing to its much greater axial length compared to its radial dimensions. Key models in this category include the infinite line source model (ILS, Ingersoll and Plass, 1948), infinite cylindrical source model (ICS, Ingersoll, 1954; Carslaw and Jaeger, 1959), finite line source model (FLS, Zeng et al., 2002), and various modified versions that incorporate considerations such as variable heat flux along the borehole length, borehole inclination, ground stratification and anisotropy, and computation efficiency improvement (Lamarche and Beauchamp, 2007a; Marcotte and Pasquier, 2009; Li and Lai, 2012; Koohi-Fayegh and Rosen, 2012; Abdelaziz et al., 2014; Cimmino, 2018; Erol and François, 2019). However, by excluding the borehole's

internal geometry and the material heat capacity, these models are unable to provide information such as the fluid temperature inside boreholes, rendering them unsuitable for dynamic simulation of ground source heat supply systems like GSHP systems.

Thermal network models are a type of analytical model aimed at analyzing heat transfer processes inside boreholes. These models are inspired by the analogous relationship between electrical and thermal currents to model the internal geometry of the borehole, including fluid in pipes and grouting material (Yang et al., 2014). In these models, the 3D structure of the borehole is discretized into slices perpendicular to the axial direction, with each slice represented by a two-dimensional (2D) thermal circuit. These circuits are interconnected through temperature nodes featuring thermal capacitances and resistances, collectively forming a thermal network. Key models in this category include the Capacity Resistance Model (CaRM, Zarrella et al., 2011), the Thermal Resistance-Capacity Model (TRCM, Bauer et al., 2011; Pasquier and Marcotte, 2012), and the Simplified Thermal Resistance-Capacity Model (STRCM, Maerefat and Minaei, 2017a). However, since these models are generally developed for individual boreholes and assume one-dimensional (1D) heat transfer in surrounding ground, they are inadequate for long-term simulations involving thermal interactions among multiple boreholes.

The third category is **composite (or hybrid) models** that simulate heat transfer both inside and outside the borehole. A common type of composite model is the analytical-numerical or semi-analytical model, where heat transfer in the surrounding ground and inside the boreholes is modelled separately using numerical and analytical methods. For example, in the model proposed by Belzile et al. (2016), the numerical part uses a 2D control volume finite difference method to solve the heat conduction in the ground, and the analytical part is composed of a multipole borehole thermal resistance to simulate the heat flow inside the borehole. In comparison, Zhang et al. (2022) adopted a numerical model to simulate the thermal behaviour of circulating fluid and grouting material inside the borehole, while heat transfer in layered ground was solved analytically using Green's function method. Analytical models can also be coupled to develop a composite model. For instance, Yang et al. (2009) integrated the variable heat flux cylinder source model for transient borehole wall temperatures with a thermal network model to assess heat transfer within the borehole, validating the model through a solar-geothermal multifunctional heat pump experiment. Alaie et al (2021) coupled the FLS model with the STRCM model to construct a transient composite model, investigating the effects of borehole spacing, layout, soil and grout properties on the outlet fluid temperature in the borehole field. Hu (2017) combined the FLS model with a thermal

network work to develop a composite analytical model for vertical borehole ground heat exchanger in layered ground. Based on the Green's function method, the segmented FLS model and composite section concept proposed by Abdelaziz et al. (2014), and a thermal network model, Guo et al. (2023) proposed a composite analytical solution addressing varying heat transfer rates for boreholes in stratified ground.

Composite models of borehole ground heat exchangers offer greater computational efficiency than numerical models. However, given the complexity of thermal performance of boreholes in stratified ground, there are still some issues in the existing literature. First, most composite models are not suitable for multiple boreholes. Ground source heat supply systems, including GSHP systems and borehole thermal energy storage, often involve borehole fields with dozens or even hundreds of boreholes that are arranged in various layouts (Gultekin et al., 2019; Cassina et al., 2022; Zhang et al., 2022). Heat transfer between adjacent boreholes will interfere with each other. These thermal interactions among boreholes occur due to temperature anomalies that develop during operation (Miglani et al., 2018). Such anomalies spatially add up over time, which has significant influences on the energy performance and efficiency of the ground source heat supply systems (Gultekin et al., 2019; Cassina et al., 2022; Li et al., 2023).

More importantly, some of the composite models are unsuitable for stratified ground conditions, where different ground layers possess varying thermophysical properties. This results in spatial and temporal variations in heat transfer within ground layers (Abdelaziz et al., 2014; Zhang et al., 2022). Ground stratification also aggravates the thermal interactions among boreholes, altering ground temperature distributions compared to homogenous ground conditions (Hu et al., 2017; Li et al., 2018). These complexities significantly impact borehole field sizing and the energy performance and efficiency of the ground source heat supply systems in complex geological formations. Despite these critical aspects, there remains a lack of models capable of accurately predicting the thermal performance of borehole fields in stratified formations, and insufficient research has been conducted on how borehole layout and ground stratification affect the thermal performance of both individual and collective boreholes.

To bridge these research gaps, a new composite analytical model tailored to evaluate the thermal performance of multiple boreholes within layered ground is established. The model divides the borehole field into two regions, utilizing a simplified thermal network model to characterize transient heat transfer inside the boreholes (Minaei and Maerefat, 2017a; Minaei and Maerefat, 2017b) and a segmented finite line source model to manage variable heat flux along the borehole depth for heat transfer outside the boreholes (Abdelaziz et al. 2014; Cimmino, 2018). The model integrates critical factors influencing heat

transfer, encompassing ground stratification, thermal interactions among boreholes, variability of heat flux along borehole depth, and flexible layouts of boreholes. Its unique capability to combine heat transfer simulations inside and outside the boreholes within a unified computational environment as a standalone module allows for seamless integration with other components of district heating and cooling networks within the TRNSYS software platform (TRNSYS, 2023). The primary objectives of the model are to (1) expedite the generation of thermal data pertinent to borehole fields in stratified ground, (2) investigate the effects of borehole layout and ground stratification on the thermal performance of individual and collective boreholes, and (3) provide a versatile tool applicable beyond GSHP systems, extending to borehole thermal energy storage, as well as district heating and cooling networks.

The structure of this paper is organized as follows. First, the composite analytical model for boreholes in stratified ground is described, detailing the establishment of a mathematical model based on the physical model. This is followed by the numerical solution of the composite model. The model is then validated through four distinct experiments, covering varied borehole quantities and ground conditions, with a focus on analyzing potential discrepancies between the simulated and measured results. Subsequently, the model is applied to investigate the thermal performance of a borehole field in three-layer ground, the effects of borehole layout and ground stratification on the outlet fluid temperature and heat injection rate are examined. Finally, a comprehensive comparison of the proposed model with existing models in the literature is conducted, and conclusions are drawn. The main innovations of this research are:

(1) development of a new composite analytical model capable of predicting the thermal performance of borehole fields in stratified ground;

(2) transient analysis of effects of thermal interactions and ground thermophysical properties on the thermal response of individual and collective boreholes;

(3) identification of boreholes that are most affected and least affected by thermal interferences of boreholes in various layout configurations;

and (4) evaluation of the significance of ground stratification on the thermal performance of borehole fields with varying borehole spacings.

2. Model development

2.1 Physical model

Fig. 1 illustrates a GSHP system coupled with borehole ground heat exchangers, facilitating the exchange of heat with the surrounding ground. Within this configuration, a set of boreholes are arranged in parallel connections within the multi-layered ground. Each borehole features an identical single U-tube, through which a heat transfer fluid circulates. Grouting material is utilized to fill the gap between the U-tube and the borehole wall, enhancing heat transfer efficiency. The fluid flows the U-tube within each borehole, either extracting or injecting heat from/to the adjacent ground.

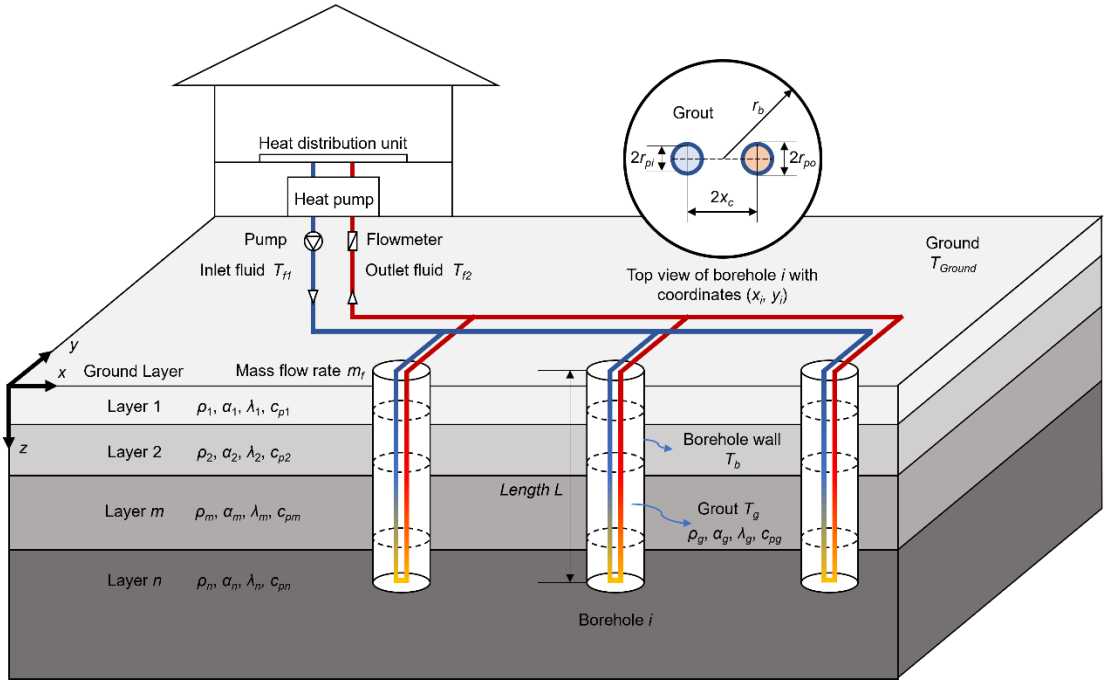

Fig. 1 Schematic showing the ground source heat pump system with multiple boreholes installed parallelly in the multi-layered ground

2.2 Mathematical model

2.2.1 Assumptions and simplifications

A composite analytical model for borehole ground heat exchangers in multi-layered ground has been developed, encompassing two fundamental parts: (1) heat transfer inside the borehole, and (2) heat transfer outside the borehole. In order to take into account both calculational efficiency and accuracy, the model is founded upon several assumptions and simplifications in a reasonable manner.

Regarding the stratified ground:

(i) The ground consists of multiple layers in the vertical direction, with the thermophysical properties of each ground layer assumed to be constant and homogeneous within the investigated temperature range (Abdelaziz et al., 2014; Hu, 2017). These properties include density ρ, thermal diffusivity α, thermal conductivity λ, and specific heat capacity c_p.

(ii) The ground is assumed to have a uniform initial temperature along the borehole's depth, denoted as T_{Ground}. It is assumed that this ground temperature is unaffected by surface climatic conditions (Cimmino, 2018; Alaie et al., 2021). This assumption is based on the fact that the temperature variations at the surface diminish a few meters below ground, rendering their influence on the thermal performance of boreholes negligible (Guo et al., 2023).

(iii) Given the complex effects of groundwater on the heat exchange between boreholes and the surrounding ground (Molina-Giraldo et al., 2011; Cai et al., 2020), the current model omits the potential influence of groundwater flow.

Concerning the boreholes:

c boreholes are standardized with uniform length L and radius r_b. In engineering practices, boreholes are buried at a certain depth below the ground surface to minimize disturbances from surface temperature changes and to provide sufficient depth for the header trench (Cimmino, 2018; Alaie et al., 2021). Considering that the buried depth (generally in meters) is much shorter compared to the borehole length (usually in hundreds of meters) and the previous assumption of an undisturbed ground temperature, the tops of the boreholes in the current model are simplified to be at the ground surface, which is commonly adopted in the literature (Abdelaziz et al., 2014; Hu, 2017; Morchio and Fossa, 2021; Zhang et al., 2022). The borehole wall temperature is represented by T_b. The location of a borehole is defined by the centre of the borehole in the ground surface plane, i.e., the $x-y$ plane. For example, the location of Borehole i can be presented by (x_i, y_i).

(ii) Each borehole has a single U-tube with legs of equal length, which is the most common configuration (Lamarche et al., 2010; Ruiz-Calvo et al., 2016; Alaie et al., 2021; Zhang et al., 2022). The length of the pipe legs matches the borehole's length L. The inner and outer radii of the pipe are represented by r_{pi} and r_{po}, respectively, with the shank spacing, denoted as x_c, indicating the distance between the borehole's centre and the pipe.

(iii) The thermophysical properties of the grouting material within the boreholes are assumed to be constant and homogeneous within the investigated temperature range (Yang et al., 2014; Hu, 2017).

These properties include density ρ_g, thermal diffusivity α_g, thermal conductivity λ_g, and specific heat capacity c_{pg}. The grout temperature is represented by T_g.

(iv) The thermophysical properties of the fluid in pipes are assumed to maintain constant within the investigated temperature range, a common assumption in the literature (Alaie et al., 2021; Zhang et al., 2022; Guo et al., 2023). These properties include density ρ_f, thermal diffusivity α_f, thermal conductivity λ_f, specific heat capacity c_{pf}, and dynamic viscosity μ_f. Additionally, the total mass flow rate of the fluid is denoted as m_f.

(v) In the current model, heat conduction is considered the primary mechanism governing heat transfer within the ground, as heat convection due to groundwater flow is not accounted for (Zeng et al., 2002). Fluid heat flow in the U-tubes is described by an assembly of interconnected resistances and capacitors (Al-Khoury and Focaccia, 2016; Minaei and Maerefat, 2017a; Minaei and Maerefat, 2017b).

Additionally, a standardized naming convention for variables involved in the model, as illustrated in Fig. 2, has been established. Herein, "X" represents a variable, which could denote temperature (T), heat flux (q), or distance between boreholes along the energy path (S). The first subscript "a" signifies the component of a borehole, such as the borehole wall (b), grout (g) or fluid (f). The second subscript "b" identifies the specific borehole, denoted by i or j. The third subscript "c" designates the ground layer, presented as m or n. The last subscript "d" denotes the section identifier, represented by u, v, or w. Any variables deviating from this naming convention are individually elucidated.

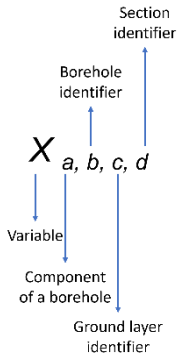

Fig. 2 Naming convention for a variable involved in the model

2.2.2 Heat transfer inside the borehole

As shown in Fig. 3, a borehole embedded within multi-layered ground is divided into a series of

segments based on the ground profile, with each segment comprising several sections. Taking Borehole i as an example, for its borehole segment within Layer m, it consists of M_m sections of equal length, calculated as follows:

$$\Delta z_{b,i,m,M_m} = \frac{Z_m - Z_{m-1}}{M_m} \quad (1)$$

where $\Delta z_{b,i,m,M_m}$ is the length of each borehole section in Layer m of Borehole i, m; Z_m and Z_{m-1} are the respective elevations for the lower and upper surfaces of Layer m, m.

Drawing on the analogy between thermal and electrical conduction, a simplified thermal network (STN) model based on Minaei and Maerefat (2017a; 2017b) is adopted to characterize the transient heat transfer inside the borehole. Fig. 3 illustrates the 2D thermal circuit representing a section within a ground layer, alongside the 3D STN model encapsulating internal sections of Borehole i within the stratified ground.

In the STN model, each section, with a thickness of $\Delta z_{b,i,m,M_m}$, comprises three thermal capacitances (two C_f and one C_g) and four thermal resistances (two R_{fg}, one R_{ff}, and one R_{gb}) corresponding to the fluid, grout, and borehole wall. The temperatures of the inlet and outlet fluids, grout, and borehole wall are represented by the temperatures at four thermal nodes. Therefore, the STN model employed in this study is characterized as a 3C4R-4 nodes model.

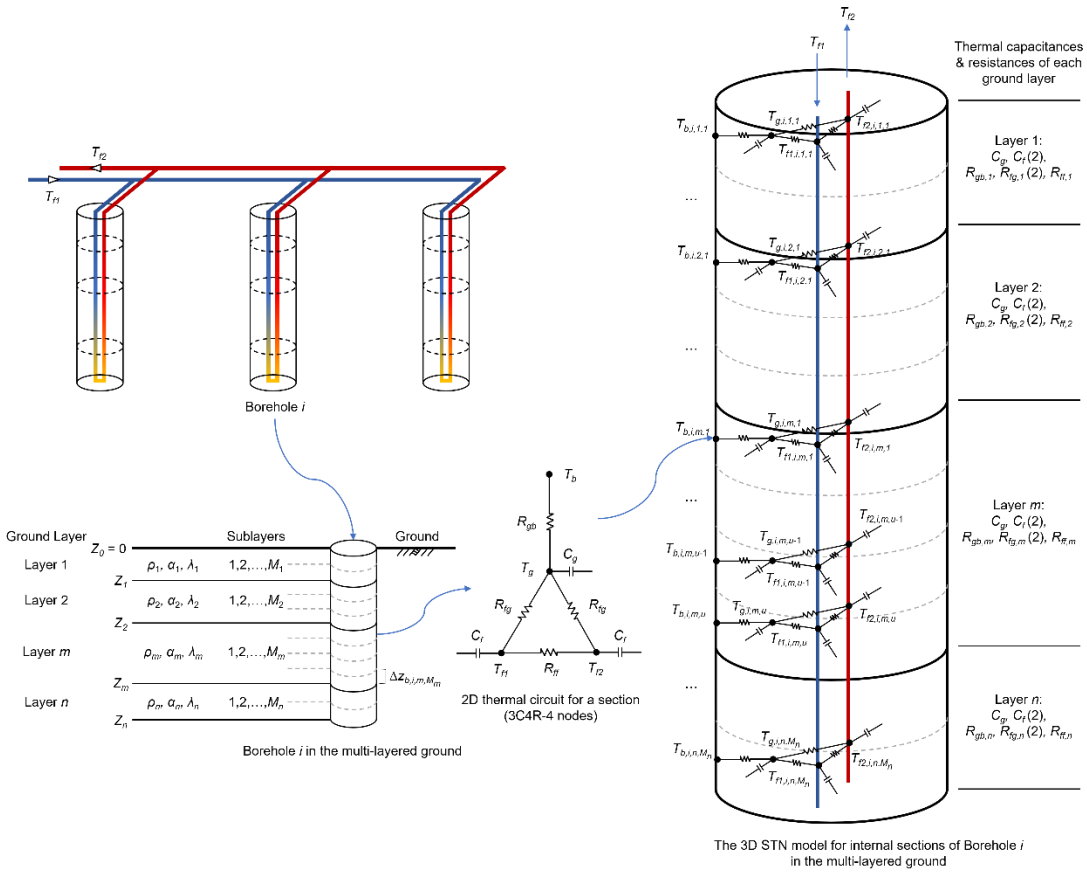

Fig. 3 Schematic showing the 2D thermal circuit for a section and the 3D STN model for internal sections of Borehole i in the multi-layered ground

(1) Thermal capacitance

For inlet and outlet fluids, the thermal capacitance of fluid C_f (J/m/K) is obtained as follows:

$$C_f = \frac{\lambda_f}{\alpha_f}\left(\pi r_{pi}^2\right) \tag{2}$$

where α_f is the fluid thermal diffusivity, m^2/s; λ_f is the fluid thermal conductivity, W/m/K; and r_{pi} is the inner radius of the pipe, m.

In the STN model, the grout is treated as a single zone, and the thermal capacitance of grout C_g (J/m/K) is calculated as follows:

$$C_g = \frac{\lambda_g}{\alpha_g}\left(\pi r_b^2 - 2\pi r_{po}^2\right) \tag{3}$$

where α_g is the grout thermal diffusivity, m^2/s; λ_g is the grout thermal conductivity, W/m/K; r_b is the borehole radius, m; and r_{po} is the outer radius of the pipe, m.

Equations (2) and (3) indicate that the thermal capacitances for thermal nodes of each section in a

borehole remain the same and are unaffected by the multiple-layered ground. This is due to the assumption that the thermophysical properties of grout and fluid are homogeneous and constant.

(2) Thermal resistance

The thermal resistance between fluid and grout R_{fb} (K·m/W) is expressed as:

$$R_{fg} = 2\left(R_b - R_{gb}\right) \tag{4}$$

in which R_{gb} is the thermal resistance between the grout and borehole wall, K·m/W, and it is calculated as:

$$R_{gb} = \frac{1}{2\pi\lambda_g}\ln\left(\frac{r_b}{r_g}\right) \tag{5}$$

where r_g is the radial location of the grout node, m, which is defined as:

$$r_g = \sqrt{\frac{r_{eq}^2 + r_b^2}{2}} \tag{6}$$

where r_{eq} is the equivalent radius, m, which is used in determining the radial location of the grout node (Lamarche and Beauchamp, 2007b). In addressing this, the two legs of the U-tube are considered as a single circular segment located at the centre of the borehole (Minaei and Maerefat, 2017a). The value of r_{eq} is defined based on the grout thermal resistance and the borehole radius (Sutton et al., 2002)

$$r_{eq} = \frac{r_b}{\exp\left(2\pi\lambda_g R_g\right)} \tag{7}$$

where R_g is the thermal resistance of grout, K·m/W. The conductive resistance of the grout cannot be calculated as straight-forward due to its irregular geometry. The value of R_g herein is expressed by (Bennet et al., 1987):

$$R_g = \frac{1}{4\pi\lambda_g}\left\{\ln\left(\frac{\lambda_1\lambda_2^{1+4\sigma}}{2\left(\lambda_2^4-1\right)^{\sigma}}\right) - \frac{\lambda_3^2\left(1-\frac{4\sigma}{\lambda_2^4-1}\right)^2}{1+\lambda_3^2\left[1+\frac{16\sigma}{\left(\lambda_2^2-\frac{1}{\lambda_2^2}\right)^2}\right]}\right\} \tag{8}$$

in which four dimensionless parameters are introduced,

$$\lambda_1 = \frac{r_b}{r_{po}} \tag{9a}$$

$$\lambda_2 = \frac{r_b}{x_c} \tag{9b}$$

$$\lambda_3 = \frac{r_{po}}{2x_c} \tag{9c}$$

$$\sigma = \frac{\lambda_g - \lambda}{\lambda_g + \lambda} \tag{10}$$

where x_c is the shaking spacing, m; and λ is the ground thermal conductivity, W/m/K, which varies with different ground layers.

It should be mentioned that the value of R_g is dependent on the thermal conductivity of each ground layer λ based on Equation (10), therefore, the values of R_{gb} and R_{fg} vary across different ground layers in the ground.

Moreover, R_b is the equivalent thermal resistance of borehole, K·m/W, representing the total thermal resistance between the circulating fluids and the borehole wall, which includes the fluid field resistance, the pipes, and the grout conductive resistances. For a single U-tube, the value of R_b can be obtained by the following equation:

$$R_b = R_g + \left(\frac{R_{conduction}+R_{convection}}{2}\right) \tag{11}$$

in which $R_{conduction}$ is the conductive resistance of the pipes, K·m/W; and $R_{convection}$ is the convective resistance of the fluid, K·m/W (Lamarche et al., 2010), and they are expressed as:

$$R_{conduction} = \frac{\ln\left(\frac{r_{po}}{r_{pi}}\right)}{2\pi\lambda_p} \tag{12}$$

$$R_{convection} = \frac{1}{2\pi r_{pi} h_{heat}} \tag{13}$$

where h_{heat} is the convective heat transfer coefficient on each pipe's interior, W/m^2/K, which can be obtained by the following equation:

$$h_{heat} = \frac{N_u \lambda_f}{2r_{pi}} \tag{14}$$

in which N_u is the Nusselt number and can be determined according to the values of Reynolds number (R_e) and Prandtl number (P_r) as follows:

(1) For laminar flow ($R_e < 2100$), there is (Hausen's formula):

$$N_u = 3.66 + \frac{0.068 R_e P_r \frac{2r_{pi}}{L}}{1+0.04\left(R_e P_r \frac{2r_{pi}}{L}\right)^{2/3}} \tag{15a}$$

(2) For transition flow ($2100 < R_e < 10000$), there is (Gnielinski's correlation):

$$N_u = \frac{\left(\frac{f}{8}\right)(R_e - 1000)P_r}{1+12.7\left(\frac{f}{8}\right)^{1/2}\left(P_r^{2/3}-1\right)} \tag{15b}$$

where f is the friction factor, and it is calculated by the following equation:

$$f = \frac{1}{(0.790 ln R_e - 1.64)^2} \tag{15c}$$

(3) For turbulent flow (R_e>10000), there is (Colburn's formula):

$$N_u = 0.023 (R_e)^{4/5} (P_r)^{1/3} \tag{15d}$$

in which,

$$R_e = \frac{\rho_f u_f 2 r_{pi}}{\mu_f} \tag{16a}$$

$$u_f = \frac{m_f}{\pi r_{pi}^2 \rho_f} \tag{16b}$$

$$P_r = \frac{\mu_f}{\alpha_f \rho_f} \tag{16c}$$

where m_f is the mass flow rate of fluid, kg/s; ρ_f is the fluid density, kg/m^3; u_f is the flow velocity of fluid, m/s; and μ_f is the fluid dynamic viscosity, kg/m/s.

Furthermore, the thermal resistance between the circulating fluids in both pipes R_{ff} (K·m/W) is equal to the interference thermal resistance R_a, and there is (Bennet et al., 1987):

$$R_{ff} = R_a = \frac{1}{\pi \lambda_g}\left[\ln\left(\frac{2\lambda_1(\lambda_2^2+1)^{\sigma}}{\lambda_2(\lambda_2^2-1)^{\sigma}}\right) - \frac{\lambda_3^2\left(1+\frac{4\sigma\lambda_2^2}{(\lambda_2^4-1)}\right)^2}{1-\lambda_3^2+\left(\frac{8\sigma\lambda_2^2\lambda_3^2(\lambda_2^4+1)}{(\lambda_2^4-1)^2}\right)}\right] \tag{17}$$

Equations (10) and (17) indicate that the value of R_{ff} varies across different ground layers.

(3) Heat balance equations

As shown in Fig. 3, the subscripts 1 and 2 denote the inlet fluid and outlet fluid, respectively. Taking Section u in Layer m of Borehole i as an example, the governing equations for the thermal nodes of inlet and outlet fluids and grout are as follows:

$$C_f \cdot \frac{\partial T_{f1,i,m,u}}{\partial t} = u_f \frac{\partial T_{f1,i,m,u}}{\partial z} + \frac{T_{f2,i,m,u} - T_{f1,i,m,u}}{R_{ff,m}} + \frac{T_{g,i,m,u} - T_{f1,i,m,u}}{R_{fg,m}} \tag{18}$$

$$C_f \cdot \frac{\partial T_{f2,i,m,u}}{\partial t} = u_f \frac{\partial T_{f2,i,m,u}}{\partial z} + \frac{T_{f1,i,m,u} - T_{f2,i,m,u}}{R_{ff,m}} + \frac{T_{g,i,m,u} - T_{f2,i,m,u}}{R_{fg,m}} \tag{19}$$

$$C_g \cdot \frac{\partial T_{g,i,m,u}}{\partial t} = \frac{T_{f1,i,m,u} - T_{g,i,m,u}}{R_{fg,m}} + \frac{T_{f2,i,m,u} - T_{g,i,m,u}}{R_{fg,m}} + \frac{T_{b,i,m,u} - T_{g,i,m,u}}{R_{gb,m}} \tag{20}$$

where T_{f1} and T_{f2} are the downward (i.e., descending) and upward (i.e., ascending) fluid temperatures, respectively, K; T_g, and T_b are the grout and borehole wall temperatures, respectively, K. In addition, at the bottom of the U-shape pipe, the temperature of the descending fluid is equal to the temperature of the ascending fluid.

2.2.3 Heat transfer outside the borehole

When investigating the heat transfer of multiple boreholes within the multi-layered ground, each borehole is conceptualized as a vertical line along the z direction, following the finite line source (FLS) model. In this approach, every section of a borehole is regarded as a finite line source, as depicted in Fig.

4, ensuring that each section of a borehole is distinctly situated within a single ground layer. To maintain a constant temperature at the ground surface, imaginary boreholes are introduced by mirroring the real boreholes around the ground surface plane (Zeng et al., 2002).

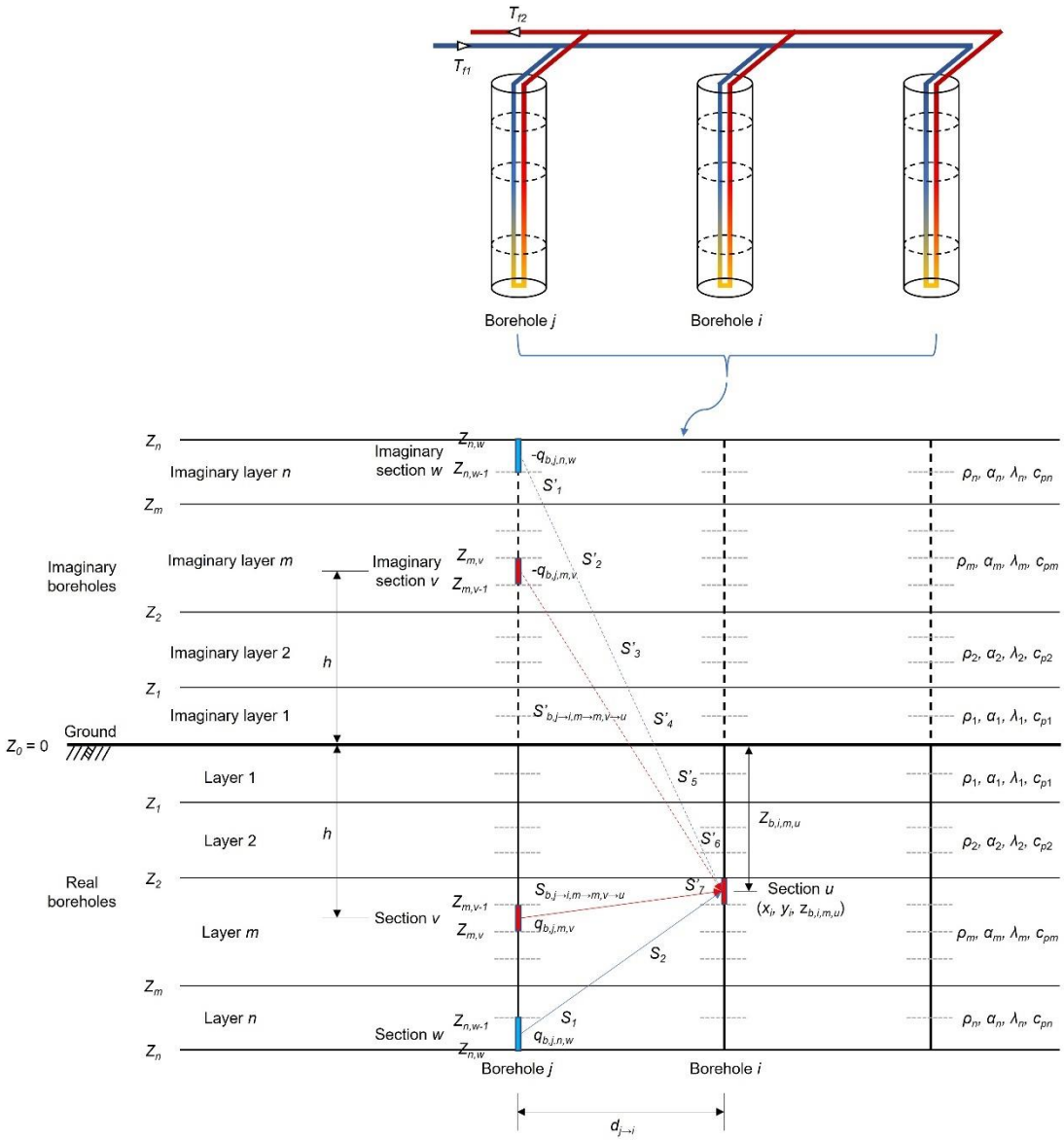

Fig. 4 Schematic showing the multiple boreholes in the multi-layered ground (after Abdelaziz et al., 2014)

As shown in Fig. 4, taking Borehole i and Borehole j as an example, with coordinates (x_i, y_i) and (x_j, y_j), respectively, their distance on the ground surface plane can be obtained as follows:

$$d_{j\to i} = d_{i\to j} = \begin{cases} r_b & i = j \\ \sqrt{(x_i - x_j)^2 + (y_i - y_j)^2} & i \neq j \end{cases} \quad (21)$$

In Fig. 4, the temperature drop/increase at Section u in Layer m of Borehole i, i.e., at the thermal node of the borehole wall, is caused by the heat extraction/injection across all sections of the real and imaginary Borehole j. Following Abdelaziz et al. (2014), this temperature variation comprises two parts to consider the differences in thermophysical properties among ground layers: (i) the primary layer, referring to the borehole section embedded within that specific layer; and (ii) the secondary layers, which encompass the borehole sections embedded within other layers. For instance, as shown in Fig. 4, concerning Section u in Layer m of Borehole i, Layer m is the primary layer, while the remaining layers constitute the secondary layers.

(1) Effect of the primary segment

Based on the FLS model, considering a constant heat flux $q_{b,j,m,v}$ (W/m), the cumulative effect of Section v in Layer m of Borehole j on Section u in Layer m of Borehole i till time t, affecting the temperature of borehole wall, can be obtained as follows (Zeng et al., 2002):

$$\Delta T_{b1,j\to i,m\to m,v\to u} = \frac{q_{b,j,m,v}}{4\pi\lambda_m} \int_{Z_{m,v-1}}^{Z_{m,v}} \left[\frac{erfc\left(S_{b,j\to i,m\to m,v\to u}/2\sqrt{\alpha_m t}\right)}{S_{b,j\to i,m\to m,v\to u}} - \frac{erfc\left(S'_{b,j\to i,m\to m,v\to u}/2\sqrt{\alpha_m t}\right)}{S'_{b,j\to i,m\to m,v\to u}} \right] dz \quad (22)$$

Equation (22) can be expressed in another way as follows:

$$\Delta T_{b1,j\to i,m\to m,v\to u} = \frac{q_{b,j,m,v}}{4\pi\lambda_m} \cdot X(t) \quad (23a)$$

$$X(t) = \int_{Z_{m,v-1}}^{Z_{m,v}} \left[\frac{erfc\left(S_{b,j\to i,m\to m,v\to u}/2\sqrt{\alpha_m t}\right)}{S_{b,j\to i,m\to m,v\to u}} - \frac{erfc\left(S'_{b,j\to i,m\to m,v\to u}/2\sqrt{\alpha_m t}\right)}{S'_{b,j\to i,m\to m,v\to u}} \right] dz \quad (23b)$$

where h is the vertical distance from the heat source to the ground surface, m; $S_{b,j\to i,m\to m,v\to u}$ is the real distance between Section v in Layer m of Borehole j and Section u in Layer m of Borehole i, m; and $S'_{b,j\to i,m\to m,v\to u}$ is the imaginary distance between the imaginary Section v in the imaginary Layer m of the imaginary Borehole j and Section u in Layer m of Borehole i, m. There are:

$$S_{b,j\to i,m\to m,v\to u} = \sqrt{{d_{j\to i}}^2 + \left(h - z_{b,i,m,u}\right)^2} \quad (24a)$$

$$S'_{b,j\to i,m\to m,v\to u} = \sqrt{{d_{j\to i}}^2 + \left(h + z_{b,i,m,u}\right)^2} \quad (24b)$$

$q_{b,j,m,v}$ is the heat flux at the borehole wall of Section v in Layer m of Borehole j, W/m, which is calculated according to the grout temperature and the borehole wall temperature:

$$q_{b,j,m,v} = \frac{T_{g,j,m,v} - T_{b,j,m,v}}{R_{gb,m}} \quad (25)$$

where $R_{gb,m}$ is the thermal resistance between grout and borehole wall in Layer m, K·m/W.

For a time-varying heat flux $q_{b,j,m,v}$, which is stepwise constant, at Section v in Layer m of Borehole j, the borehole wall temperature variation at Section u in Layer m of Borehole i at time t is obtained from the temporal superposition of the FLS solution (Cimmino, 2018):

$$\Delta T_{b1,j\to i,m\to m,v\to u}(t_k) = \frac{q_{b,j,m,v}(t_{k'})}{4\pi\lambda_m}\sum_{k'=1}^{k}[X(t_k - t_{k'-1}) - X(t_k - t_{k'})]$$

$$= \frac{1}{4\pi\lambda_m}\left[\frac{T_{g,j,m,v}(t_{k'}) - T_{b,j,m,v}(t_{k'})}{R_{gb,m}}\right]\sum_{k'=1}^{k}[X(t_k - t_{k'-1}) - X(t_k - t_{k'})] \quad (26)$$

where k is the time step index, and $q_{b,j,m,v}(t_{k'})$ is the constant heat flux over the period $t_{k'-1} < t \leq t_{k'}$, W/m.

Based on the spatial supervision, the effect of all sections (from v =1 to $v = M_m$) in Layer m of Borehole j on Section u in Layer m of Borehole i, affecting the temperature of borehole wall, can be calculated by the following equation:

$$\Delta T_{b1,j\to i,m\to m,u} = \sum_{v=1}^{v=M_m}\Delta T_{b1,j\to i,m\to m,v\to u} \quad (27)$$

Therefore, the total effect of all sections in Layer m of all boreholes (from $j = 1$ to $j = N$) on Section u in Layer m of Borehole i, affecting the temperature of borehole wall, can be obtained:

$$\Delta T_{b1,i,m\to m,u} = \sum_{j=1}^{j=N}\Delta T_{b1,j\to i,m\to m,u} = \sum_{j=1}^{j=N}\sum_{v=1}^{v=M_m}\Delta T_{b1,j\to i,m\to m,v\to u} \quad (28)$$

where N is the total number of boreholes.

(2) Effect of the secondary segment

Based on the composite section concept introduced by Abdelaziz (2014), the thermal properties of each layer along the energy path from the specific source point toward the observation section, i.e., the thermal node of the borehole wall, are used to evaluate the composite properties of the path. This involves consolidating three thermal properties of the ground layer: density ρ, thermal conductivity λ, and specific heat capacity c_p, into a real single composite section as follows:

$$\rho_{comp} = \sum_{k=1}^{k=l}\frac{S_k\cdot\rho_k}{\sum_{k=1}^{k=l}S_k} \quad (29)$$

$$\frac{1}{\lambda_{comp}} = \sum_{k=1}^{k=l}\frac{\left(S_k/\sum_{k=1}^{k=l}S_k\right)}{\lambda_k} \quad (30)$$

$$c_{pcomp} = \sum_{k=1}^{k=l}\frac{c_{pk}\cdot S_k\cdot\rho_k}{\sum_{k=1}^{k=l}(S_k\cdot\rho_k)} \quad (31)$$

where ρ_{comp} is the composite density, kg/m^3; λ_{comp} is the composite thermal conductivity, W/m/K;

451 c_{pcomp} is the composite specific heat capacity, J/kg/K; k is the layer identifier in the energy path, and
452 l is the number of layers in the energy path.

453 Using the thermal properties of the composite section, the composite thermal diffusivity α_{comp} (m^2/s)
454 can be obtained as follows:

455 $$\alpha_{comp} = \frac{\lambda_{comp}}{\rho_{comp} \cdot c_{pcomp}} \tag{32}$$

456 Similarly, the imaginary composite density ρ'_{comp}, imaginary composite thermal conductivity λ'_{comp},
457 imaginary composite specific heat capacity c'_{pcomp}, and imaginary composite thermal diffusivity α'_{comp}
458 can be obtained.

459 Based on the FLS model, for a constant heat rate $q_{b,j,n,w}$, the effect of Section w in Layer n of
460 Borehole j at Section u in Layer m of Borehole i on the temperature of borehole wall can be
461 obtained as follows (Zeng et al., 2002):

462 $$\Delta T_{b2,j\to i,n\to m,w\to u}(t) = \frac{q_{b,j,n,w}}{4\pi} \cdot Y(t) \tag{33a}$$

463 in which,

464 $$Y(t) = \int_{Z_{n,w-1}}^{Z_{n,w}} \left[\frac{erfc\left(\sum_{k=1}^{k=l} S_k / 2\sqrt{\alpha_{comp} t}\right)}{\lambda_{comp} \cdot \sum_{k=1}^{k=l} S_k} - \frac{erfc\left(\sum_{k=1}^{k=l} S'_k / 2\sqrt{\alpha'_{comp} t}\right)}{\lambda'_{comp} \cdot \sum_{k=1}^{k=l} S'_k} \right] dz \tag{33b}$$

465 where the distances S_k and S'_k (m) can easily be calculated using trigonometry according to the
466 coordinates of thermal nodes of each section of Borehole j and Borehole i, and $q_{b,j,n,w}$ is the heat flux
467 at the borehole wall of Section w in Layer n of Borehole j, W/m, which is calculated according to the
468 grout temperature and the borehole wall:

469 $$q_{b,j,n,w} = \frac{T_{g,j,n,w} - T_{b,j,n,w}}{R_{gb,n}} \tag{34}$$

470 where $R_{gb,n}$ is the thermal resistance between grout and borehole wall in Layer n, K·m/W.

471 For a time-varying heat flux $q_{b,j,n,w}$, which is stepwise constant, at Section w in Layer n of
472 Borehole j, the borehole wall temperature variation at Section u in Layer m of Borehole i at time t
473 is obtained from the temporal superposition of the FLS solution (Cimmino, 2018):

474 $$\Delta T_{b2,j\to i,n\to m,w\to u}(t_k) = \frac{1}{4\pi} \left[\frac{T_{g,j,n,w}(t_{k'}) - T_{b,j,n,w}(t_{k'})}{R_{gb,n}} \right] \sum_{k'=1}^{k} [Y(t_k - t_{k'-1}) - Y(t_k - t_{k'})] \tag{35}$$

475 where $q_{b,j,m,v}(t_{k'})$ is the constant heat flux over the period $t_{k'-1} < t \le t_{k'}$, W/m.

476 Based on the spatial superposition, the effect of all sections (from w =1 to $w = M_n$) in Layer n of
477 Borehole j at Section u in Layer m of Borehole i on the temperature of borehole wall can be

calculated by the following equation:

$$\Delta T_{b2,j\to i,n\to m,u} = \sum_{w=1}^{w=M_n} \Delta T_{b2,j\to i,n\to m,w\to u} \tag{36}$$

The total effect of all sections in the other layers ($n \neq m$) of all boreholes (from $j = 1$ to $j = N$) at Section u in Layer m of Borehole i on the temperature of borehole wall can be obtained:

$$\Delta T_{b2,i,n\to m,u} = \sum_{j=1}^{j=N} \sum_{n=1}^{n\neq m} \Delta T_{b2,j\to i,n\to m,u} = \sum_{j=1}^{j=N} \sum_{n=1}^{n\neq m} \sum_{w=1}^{w=M_n} \Delta T_{b2,j\to i,n\to m,w\to u} \tag{37}$$

Therefore, taking the effects of the primary and secondary segments into account, the temperature of borehole wall of Section u in Layer m of Borehole i, $T_{b,i,m,u}$ (K) can be expressed as follows:

$$T_{b,i,m,u} = T_{ground} + \Delta T_{b1,i,m\to m,u} + \Delta T_{b2,i,n\to m,u} \tag{38}$$

The borehole wall temperature T_b is the link between the heat transfer inside the borehole and the heat transfer outside the borehole.

3. Numerical solution

The present study employs the Lax-Wendroff method (Lax and Wendroff, 1960), an explicit time integration method for solving hyperbolic partial differential equations through finite differences. Using this method, it can compute the inlet and outlet fluid temperatures, as well as the grout temperature at the nodes of the thermal network at a certain time $(n+1)$ depending on the preceding temperature values (n). Equations (18) to (20) can be discretized as follows:

$$T_{f1,i,m,u}^{n+1} = T_{f1,i,m,u}^{n} + \frac{\Delta t \cdot u_f}{2\Delta z_{b,i,m,M_m}}\left[\left(T_{f1,i,m,u-1}^{n} - T_{f1,i,m,u+1}^{n}\right) + \frac{\Delta t \cdot u_f}{\Delta z_{b,i,m,M_m}}\left(T_{f1,i,m,u+1}^{n} - 2T_{f1,i,m,u}^{n} + T_{f1,i,m,u-1}^{n}\right)\right] + \frac{\Delta t}{C_f}\left[\frac{T_{f2,i,m,u}^{n} - T_{f1,i,m,u}^{n}}{R_{ff,m}} + \frac{T_{g,i,m,u}^{n} - T_{f1,i,m,u}^{n}}{R_{fg,m}}\right] \tag{39}$$

$$T_{f2,i,m,u}^{n+1} = T_{f2,i,m,u}^{n} + \frac{\Delta t \cdot u_f}{2\Delta z_{b,i,m,M_m}}\left[\left(T_{f2,i,m,u-1}^{n} - T_{f2,i,m,u+1}^{n}\right) + \frac{\Delta t \cdot u_f}{\Delta z_{b,i,m,M_m}}\left(T_{f2,i,m,u+1}^{n} - 2T_{f2,i,m,u}^{n} + T_{f2,i,m,u-1}^{n}\right)\right] + \frac{\Delta t}{C_f}\left[\frac{T_{f1,i,m,u}^{n} - T_{f2,i,m,u}^{n}}{R_{ff,m}} + \frac{T_{g,i,m,u}^{n} - T_{f2,i,m,u}^{n}}{R_{fg,m}}\right] \tag{40}$$

$$T_{g,i,m,u}^{n+1} = T_{g,i,m,u}^{n} + \frac{\Delta t}{C_g}\left[\frac{T_{f1,i,m,u}^{n} - T_{g,i,m,u}^{n}}{R_{fg,m}} + \frac{T_{f2,i,m,u}^{n} - T_{g,i,m,u}^{n}}{R_{fg,m}} + \frac{T_{b,i,m,u}^{n} - T_{g,i,m,u}^{n}}{R_{gb,m}}\right] \tag{41}$$

The time-step Δt (s) used for the calculations is dependent on the spatial discretization of the simulation, and its maximum value is fixed by the Courant-Friedrichs-Lewy (CFL) condition (Ruiz-Calvo et al., 2015):

$$\frac{\Delta t}{\Delta t_{max}} = \mathrm{CFL} \leq 1 \tag{42a}$$

in which,

$$\Delta t_{max} \leq \frac{min[\Delta z_{b,i,m,M_m}]}{u_f} \tag{42b}$$

where $min[\Delta z_{b,i,m,M_m}]$ denotes the minimum length of the section in a borehole.

For the integrations $X(t)$ and $Y(t)$ in Equation (23b) and Equation (33b), respectively, their values are obtained using the trapezoidal rule. The accuracy and computation efficiency for the integration rely on the number of intervals for the trapezoidal rule, as well as the time step. In this study, the number of intervals is taken as 50, a choice that yields satisfactory accuracy and computation efficiency.

As shown in Fig. 5, the proposed composite model has been programmed in Fortran and implemented as a component within the TRNSYS software (TRNSYS, 2023), designated as Type 255.

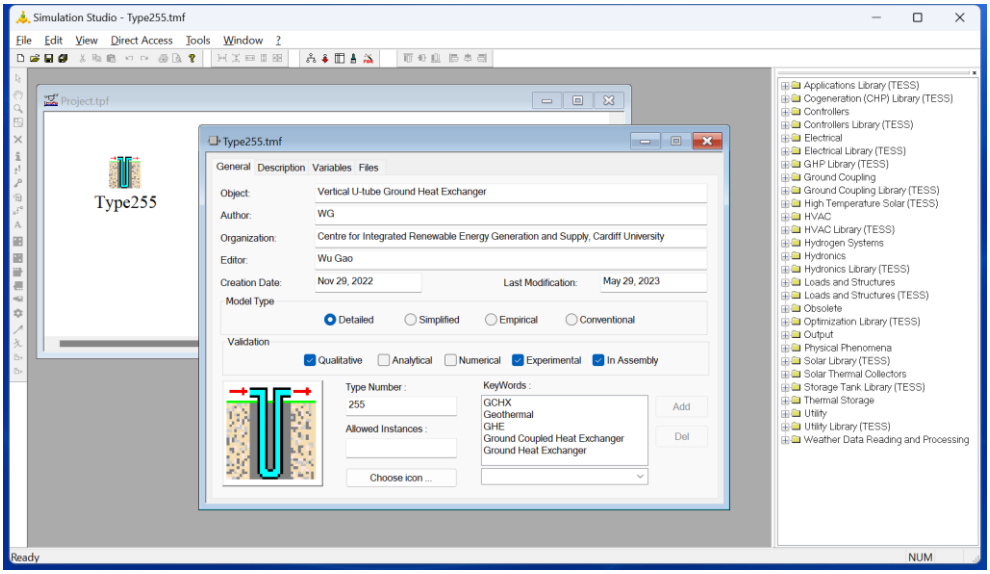

Fig. 5 User-developed borehole model (Type 255) in TRNSYS

To establish a simulation and derive meaningful outputs, it is essential to have a thorough understanding of the requisite model parameters and inputs. Fig. 6 illustrates the hierarchical relationships among the model parameters, inputs, the model itself, and the outputs. Moreover, the completeness of a simulation necessitates supplementary running information, including simulation time step, start time, and stop time. Subsequent model validation and application are conducted in the TRNSYS software environment.

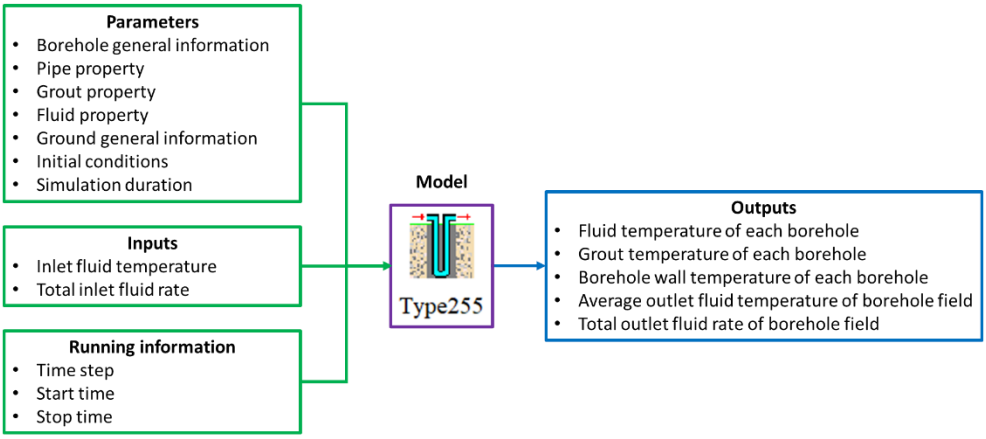

Fig. 6 Hierarchical relationships within the proposed model

4. Model validations

Given that the composite analytical model in this study encompasses both internal and external heat transfer of boreholes and aims to predict the thermal performance of a borehole field in stratified ground, comprehensive validation efforts have been undertaken. Four distinct experiments from the literature (Beier et al., 2011; Hu et al., 2017; Chen et al., 2018; Chen et al., 2021; Li et al., 2018; Li et al., 2019) were leveraged for this purpose, spanning diverse borehole quantities and ground conditions. These experiments meticulously document geologic conditions, ground properties, and borehole and fluid characteristics, which are detailed in the **Supplementary Materials**.

In this study, the root mean square error (RMSE), mean absolute error (MAE) and mean absolute percentage error (MAPE), as defined in the following equations, are employed to quantify the alignment between the simulated results (SR) and the measured results (MR) of temperature for the entire duration in each validation case.

$$\mathrm{RMSE} = \sqrt{\frac{\sum_{i=1}^{n}\left(T_{i,\mathrm{MR}} - T_{i,\mathrm{SR}}\right)^2}{n}} \tag{43a}$$

$$\mathrm{MAE} = \frac{1}{n}\sum_{i=1}^{n}\left|T_{i,\mathrm{MR}} - T_{i,\mathrm{SR}}\right| \tag{43b}$$

$$\mathrm{MAPE} = \frac{1}{n}\sum_{i=1}^{n}\left|\frac{T_{i,\mathrm{MR}} - T_{i,\mathrm{SR}}}{T_{i,\mathrm{MR}}}\right| \times 100\% \tag{43b}$$

where n is the number of sample data points; $T_{i,\mathrm{MR}}$ is the ith measured result of temperature, ℃; and $T_{i,\mathrm{SR}}$ is the ith simulated result of temperature obtained from the proposed composite analytical model, ℃.

4.1 Background information of four validation cases

4.1.1 One borehole in single-layered ground

Beier et al. (2011) carried out a thermal response test within a large laboratory "sandbox", containing a borehole outfitted with a single U-tube. Notably, the pipe was encased within a horizontal aluminium pipe before being buried in the sandbox. To ensure effective heat transfer between the pipe and the surrounding sand, the aluminium pipe was filled with bentonite grout. Over the course of the 51-hour experiment, inlet and outlet temperatures, along with varied water flow rates, were recorded. This experimental setup is equivalent to the scenario of a single borehole in homogenous ground.

4.1.2 One borehole in three-layered ground

Hu (2017) conducted a thermal response test in a borehole under a constant flow rate condition. The vertical borehole, with a length of 63 m, penetrated three distinct ground layers: backfill soil, clay, and fine sand, with respective thicknesses of 20 m, 18 m, and 25 m. During the 43-hour experiment, inlet and outlet fluid temperatures from the signle U-tube were measured. This experiment setup corresponds to the scenario of a single borehole in stratified ground.

4.1.3 Sixteen boreholes in single-layered ground

In the absence of direct experimental data concerning multiple boreholes, the accuracy of the model for multiple boreholes can be verified via comparison with results derived from a single borehole experiment (Chen et al., 2021). In this case, an in-situ test of a single borehole under a fixed flow rate performed by Chen et al. (2018) was employed. A borehole field comprising 16 boreholes within a single-layered ground was designed, identical to the setup in Chen et al. (2021). These 100-m-long boreholes were arranged in a square layout, with a lateral and longitudinal spacing of 4 m between adjacent boreholes. This validation case is equivalent to the scenario of multiple boreholes in homogenous ground.

4.1.4 Two boreholes in two-layered ground

Li et al. (2018) and Li et al. (2019) experimentally investigated the thermal performance of vertical ground heat exchangers using an indoor testing box filled with sand and clay. The upper layer was sand with a thickness of 3.0 m, while the lower layer was clay with a thickness of 3.25 m. Test 1 from the series of experiments in Li et al. (2019) was selected for the validation of the present model. Throughout

this test, heated water circulated at a constant flow rate within two parallel U-shape copper pipes, spaced 0.5 m apart, transferring heat to the surrounding ground. Inlet and outlet water temperatures were recorded. This experiment setup corresponds to the scenario of a borehole array in stratified ground.

4.2 Comparison of results

A comparative analysis between the simulated and experimental results from Beier et al. (2011) is presented in Fig. 7(a). The simulated outlet fluid temperatures exhibit a consistent trend with the experimental results, though with slightly higher values. The RMSE, MAE, and MAPE are 0.68 ℃, 0.50 ℃, and 1.39%, respectively. By the end of the experiment, a temperature difference of 0.48°C had accumulated.

In Fig. 7(b), the outlet fluid temperature predicted by the present model is compared with both the experimental and analytical results of Hu (2017). The simulated results align well with Hu's experimental data, with the RMSE of 0.29 ℃, the MAE of 0.17 ℃, and the MAPE of 0.75%. A deviation of 0.14 ℃ was observed at the end of the experiment.

Fig. 7(c) contrasts the average outlet fluid temperature of the borehole field, as calculated by the proposed model, with that of the single borehole experiment in Chen et al. (2021). The simulated results of the borehole field consistently reflect the measured pattern from the experiment, with the RMSE and MAE of 0.60 ℃ and 0.47 ℃, and the MAPE of 2.02%.

Compared to the prior three cases, the experimental setup in Li et al. (2019) included the complexities associated with multi-pipe interference and ground stratification. Fig. 7(d) illustrates the simulated outlet fluid temperature alongside the experimental inlet and outlet fluid temperatures. The RMSE of 0.27 ℃, MAE of 0.22 ℃ and MAPE of 0.87% indicate a good agreement with the experimental data.

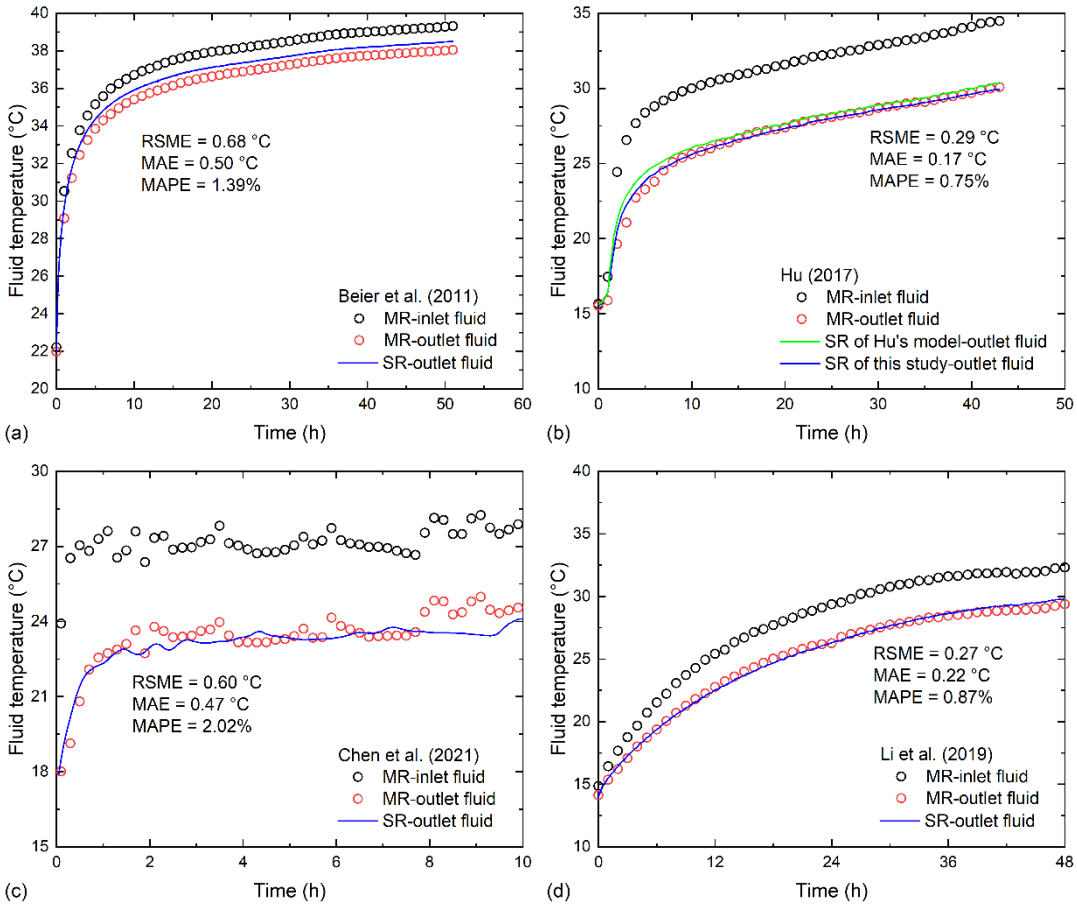

Fig. 7 Comparison of measured results (MR) and simulated results (SR) in (a) Beier et al. (2011), (b) Hu (2017), (c) Chen et al. (2021), and (d) Li et al. (2019)

The discrepancies between the simulated and measured results can be mainly summarized as follows: (1) Unmodelled physical phenomena. For instance, in the validation case of Beier et al. (2011), the presence of the aluminium pipe was not included in the simulation. Due to aluminum's high thermal conductivity (237.0 W/m/K) and thermal diffusivity, which are significantly greater than those of the surrounding wet sand and grout, the aluminum pipe facilitated more efficient heat dissipation to the surrounding ground. As a result, the measured outlet fluid temperatures were lower than the simulated values, where the thermal transfer effect of the aluminum pipe was not considered. (2) Availability of thermophysical parameters. In some cases, certain parameters were not explicitly provided and had to be inferred from similar literature and database. For example, the ground parameters from Hu (2017) were employed in the simulations of Beier et al. (2011). (3) Simplifications in calculating the temperature response outside the borehole. The proposed model calculates the temperature response at a certain point in the ground by superposing the contributions of all the segments. The temperature response of heat

exchanger segments outside the segmental source layer was obtained using composite thermal properties, following Abdelaziz et al. (2014). However, for stratified ground scenarios, this method may not fully satisfy the heat transfer governing equation (Zhang et al., 2022). (4) Simplifications of heat transfer inside the borehole. In the proposed model, the heat transfer process inside the borehole is treated as steady and is theoretically modelled using an equivalent thermal network (Yang et al., 2009). However, it takes time for the heat transfer inside the borehole to transfer from unsteady to steady-state conditions, which could explain the higher simulated outlet fluid temperatures compared to experimental data during the first 8 hours of the thermal response test conducted by Hu (2017). (5) Other limitations of the model, such as the neglect of geothermal gradient and vertical heat conduction through the grouting material, and the assumption that thermophysical parameters are independent of temperature.

Drawing upon comprehensive validation cases across various borehole quantities and ground conditions, the proposed model exhibits consistent simulation results relative to experimental results. Additionally, the proposed model demonstrates satisfactory computation efficiency. For example, when simulating the thermal response test conducted by Hu (2017) on the same workstation (Windows 11, 13th Gen Intel Core i7, and 16.0 GB RAM), the proposed analytical model significantly outperformed the earlier numerical model (a finite element model) developed by Gao et al. (2023b). The numerical model required approximately 15 minutes to complete, whereas the analytical model completed the simulation in less than 1 minute. Thus, the composite analytical model presented in this study is well-suited for investigating the thermal performance of borehole arrays in various layouts within the stratified ground.

5. Model applications

5.1 Borehole layout and ground stratification

In this study, a series of long-term simulations spanning 60 days are undertaken on a borehole field operating in cooling mode. The primary objective is to investigate the effects of borehole layout and ground stratification on both the outlet fluid temperature and the heat injection rate. The heat injection rate of a borehole field or borehole P (kW) can be calculated as:

$$P = \frac{m_f c_{pf} (T_{in} - \bar{T}_{out})}{1000} \tag{44}$$

in which,

$$\bar{T}_{out} = \begin{cases} \frac{\sum_{i=1}^{N} T_{f2,i,1,1}}{N} & for\ a\ borehole\ field \\ T_{f2,i,1,1} & for\ a\ borehole \end{cases} \quad (45)$$

where $T_{f2,i,1,1}$ is the outlet fluid temperature of Borehole i, ℃; $\bar{T}_{out}$ is the average outlet fluid temperature of the borehole field, ℃; and T_{in} is the inlet fluid temperature, ℃.

The borehole field comprises 16 boreholes, each equipped with a single U-tube. The ground profile in Hu (2017) is adopted, featuring three ground layers consisting of backfill soil, clay, and fine sand from the ground surface to a depth of 63 m. The thermophysical properties of these ground layers, as well as the grouting material, are detailed in Table 1. Consistent with the parameters specified in Hu (2017), the borehole and U-shape pipe specifications are outlined in Table 2. Throughout the simulations, the inlet water temperature remains constant at 30.0 ℃, with a total mass flow rate of 3.2 kg/s. The initial and undisturbed ground temperature is 15.5 ℃, as documented by Hu (2017).

To assess the influence of borehole layout, three layout configurations, that is, square, L-shape, and linear, are designed based on the studies by Gultekin et al. (2019), Alaie et al. (2021), and Cassina et al. (2022), as depicted in Fig. 8. Each layout is characterized by uniform lateral and longitudinal distances between adjacent boreholes, denoted as *d* (m). The range of spacing between adjacent boreholes is from 1 m to 4 m.

Furthermore, to study the impact of ground stratification, a homogenous ground extending to a depth of 63 m is assumed. The thermophysical properties of this homogenous ground layer, including density, specific heat capacity, and thermal conductivity, are determined using the weighted average method. In this method, the thickness of each ground layer is used as the weight coefficient, multiplied by the respective thermophysical parameters of the ground layers (Jin et al., 2020). Consequently, the thermophysical properties of the homogenous ground are calculated and listed in Table 1. It can be seen from the table that the thermal diffusivity of the three ground layers, ranked from highest to lowest, is: Layer 1 (backfill soil) > Layer 3 (fine sand) > Layer 2 (Clay). Additionally, the thermal diffusivity of the homogenous ground is comparable to that of Layer 3.

Table 1 Physical parameters of ground layers

Ground conditions		Depth z (m)	Density ρ (kg/m^3)	Specific heat capacity c_p (J/kg/K)	Thermal conductivity λ (W/m/K)	Thermal diffusivity α (m^2/s)
Stratified	1 - Backfill soil	0-20	1880	910	2.12	1.24e-6

ground	2 - Clay	20-38	1680	2225	1.20	3.21e-7
	3 - Fine sand	38-63	1980	1400	1.61	5.81e-7
Homogenous ground		0-63	1862.54	1480.16	1.65	5.99e-7
Grout		0-63	1847	1512	1.50	5.37e-7

Table 2 Parameters of the borehole and U-shape pipe

Parameter	Symbol	Value	Unit
Borehole length	L	63	m
Fixed mass flow rate of water	m_f	3.2	kg/s
Density of water	ρ_f	1000	kg/m^3
Dynamic viscosity of water	μ_f	0.001	kg/m/s
Specific heat capacity of water	c_{pf}	4200.0	J/kg/K
Thermal conductivity of water	λ_f	0.599	W/m/K
Borehole radius	r_b	0.070	m
Pipe outer radius	r_{po}	0.016	m
Pipe inner radius	r_{pi}	0.013	m
Shank spacing	x_c	0.030	m
Thermal conductivity of pipe	λ_p	0.450	W/m/K

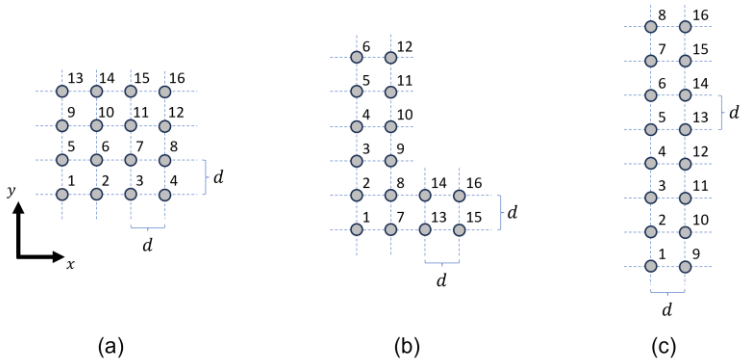

(a) (b) (c)

Fig. 8 Schematics of borehole's layout: (a) square configuration, (b) L-shape configuration, and (c) linear configuration

5.2 Results

5.2.1 Effects of borehole layout on average outlet fluid temperature and heat injection rate of borehole field

Fig. 9(a) displays the average outlet fluid temperature across different borehole layouts and spacings. As observed in the figure, the average outlet fluid temperature gradually increases over time. This temperature elevation results from significant thermal interactions among boreholes, where heat injected into the ground raises the temperature within the borehole field (Jin et al., 2020; Alaie et al., 2021;

Cassina et al., 2022; Zhang et al., 2022). For comparison, the outlet fluid temperature of a single borehole is also plotted in Fig. 9(a). Across all layout configurations, the average outlet fluid temperatures converge towards that of the one borehole scenario as the borehole spacing extends to 4 m. This indicates that the effect of borehole layout, i.e., thermal interference of boreholes, on the thermal performance of the borehole field decreases when the borehole spacing is sufficiently wide (Alaie et al., 2021). In scenarios involving closely arranged boreholes, such as those with a 1-m spacing, the impact of thermal interaction becomes more pronounced. In these cases, heat retention within the borehole field leads to substantially higher outlet fluid temperature compared to that of the one borehole scenario, consistent with the numerical findings in the literature (Zhang et al., 2022). In addition, the average outlet fluid temperature for the square layout configuration slightly exceeds that of the L-shape and linear layout configurations, which aligns with the observations of Alaie et al. (2021). By Day 60, all three layouts in this analysis converge to an average outlet fluid temperature of approximately 29.97 ℃, approaching the inlet fluid temperature of 30 ℃.

Fig. 9(b) depicts the evolution of the heat injection rate of the borehole field across three layout configurations, as well as the heat injection rate for 16 times that of a single borehole. The figure shows a noticeable decline in the heat injection rate for each layout configuration over time, which can be attributed to the progressive rise in the average outlet fluid temperature (Zhang et al., 2022). For instance, in the borehole field with a 1-m spacing, the square layout exhibits the lowest heat injection rate, followed by the L-shape and linear layouts. The heat injection rate in these configurations decreases from 6.39-6.96 kW on Day 10 to 0.36-0.42 kW on Day 60 in this analysis. In contrast, for the case of 16 times the single borehole, the heat injection rate decreases from 14.00 kW on Day 10 to 8.25 kW on Day 60. The significant difference between the heat injection rate of the borehole field and that of a single borehole multiplied by 16 highlights the substantial thermal performance distinctions caused by the intricate thermal interactions and interferences with the borehole field. These findings agrees with the numerical results obtained by Jin et al. (2020), Zhang et al. (2022), and Gultekin et al. (2019). Hence, the significance of the proposed model in this study is underscored by these observations.

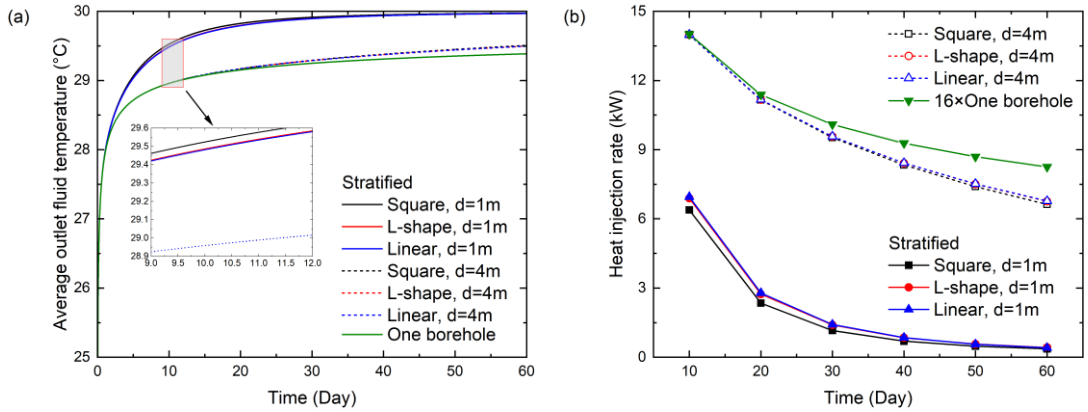

Fig. 9 Effects of borehole layout on (a) average outlet fluid temperature and (b) heat injection rate across different borehole layout configurations and distances in stratified ground

5.2.2 Effects of borehole layout on fluid temperature and heat injection rate of representative boreholes

Fig. 10 illustrates the outlet fluid temperature contours for individual boreholes (BHs) in stratified ground with two spacings, 1 m and 4 m, across three layout configurations on Day 60. In the square layout configuration (Fig. 10(a) and Fig. 10(b)), boreholes with identical outlet temperatures display biaxial symmetry. Analyzing the thermal performance of individual boreholes shows that those located at the core of the borehole field (i.e., BHs 6, 7, 10, and 11) exhibit the highest outlet temperatures due to ground thermal retention and borehole thermal interference. Conversely, boreholes at the four corners of the field (i.e., BHs 1, 4, 13, and 16) show the lowest values. This indicates that BHs 6, 7, 10 and 11 are most affected by the surrounding boreholes' heat flow, while BHs 1, 4, 13, 16 experience the least impact by the other boreholes, consistent with the findings of Zhang et al. (2022) and Belzile et al. (2016). At a 1-m spacing, the outlet temperature of BHs 6, 7, 10, and 11 reach 30.24 ℃, exceeding the inlet temperature of 30 ℃ in this analysis, while BHs 1, 4, 13, and 16 register 29.72 ℃, indicating heat dissipation to the surroundings. As borehole spacing increases, thermal interference decreases (Gultekin et al., 2019; Alaie et al., 2021; Cassina et al., 2022; Bandeira Neto et al., 2023). At a 4-m spacing, the outlet temperatures of core boreholes and corner boreholes drop to 29.55 ℃ and 29.46 ℃, respectively, both below the inlet temperature of 30 ℃.

In the L-shape layout configuration (Fig. 10(c) and Fig. 10(d)), the borehole with the highest outlet fluid temperature is BH 8, located at the inner corner of the layout, where it is most affected by surrounding boreholes in this analysis. Conversely, BH 1, situated at the outer corner, has the lowest

temperature due to minimal thermal interaction. With a 1-m spacing, the outlet temperature of BH 8 reaches 30.26 ℃, higher than the inlet temperature of 30 ℃, while that of BH 1 is 29.73 ℃, which is about 0.53 ℃ lower than the highest value. Increasing the spacing to 4 m reduces the outlet temperatures of BH 8 and BH 1 to 29.55 ℃ and 29.46 ℃, respectively, with a temperature difference of less than 0.10 ℃.

Fig. 10(e) and Fig. 10(f) present the outlet fluid temperature contours for individual boreholes in the linear layout configuration. Boreholes with identical outlet temperatures exhibit biaxial symmetry. For both spacings in this analysis, BHs 2, 7, 10, and 15, located in the second-row inward along the x direction, are the most affected, producing the highest outlet temperatures. In contrast, BHs 1, 8, 9, and 16, positioned in the outermost rows, are the least affected, producing the lowest temperatures. At a 1-m spacing, the outlet temperatures of BHs 2, 7, 10, and 15 reach 30.06 ℃, exceeding the inlet temperature, while BHs 1, 8, 9, and 16 record 29.80 ℃. In the 4-m spacing scenario, the outlet fluid temperatures of BHs 2, 7, 10 and 15 and BHs 1, 8, 9, and 16 are similar, which are 29.51 ℃ and 29.48 ℃, respectively.

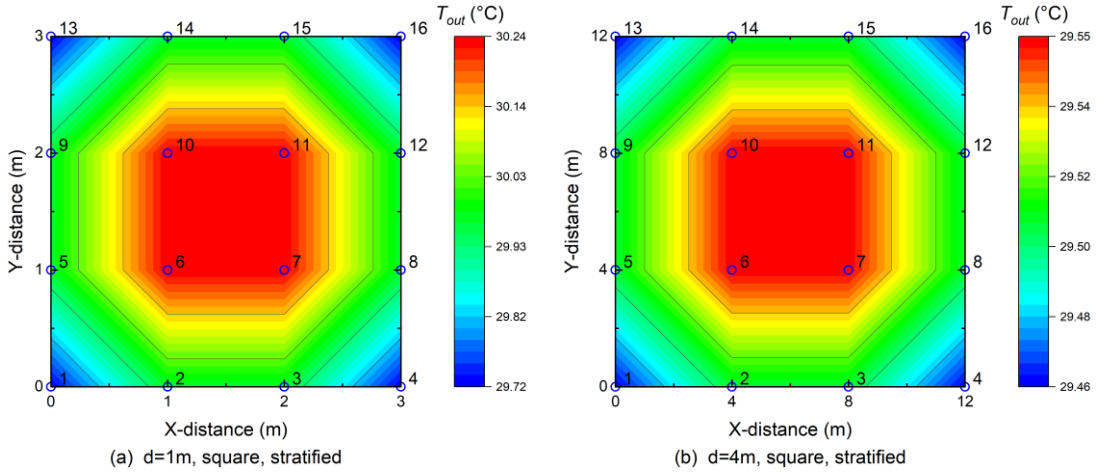

(a) d=1m, square, stratified (b) d=4m, square, stratified

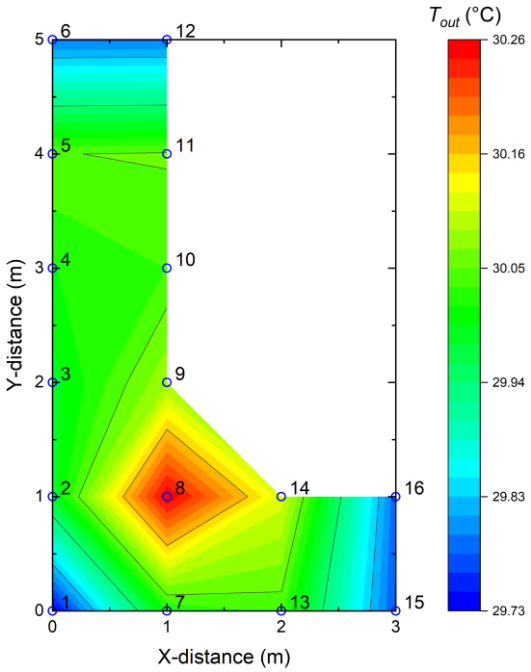

(c) d=1m, L-shape, stratified

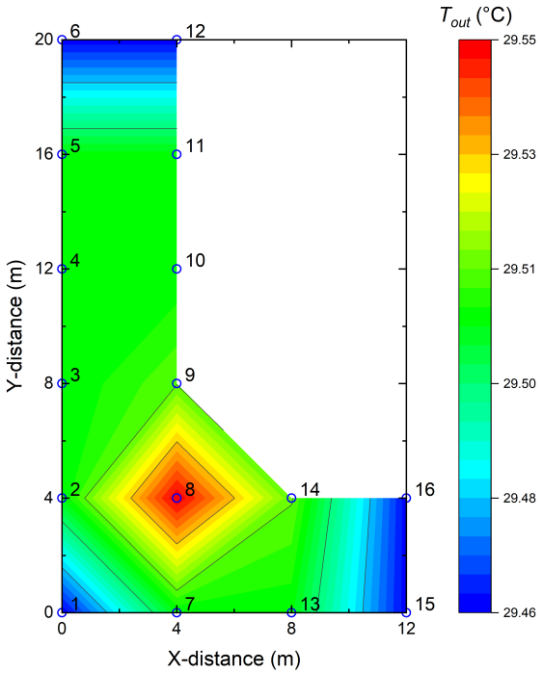

(d) d=4m, L-shape, stratified

751

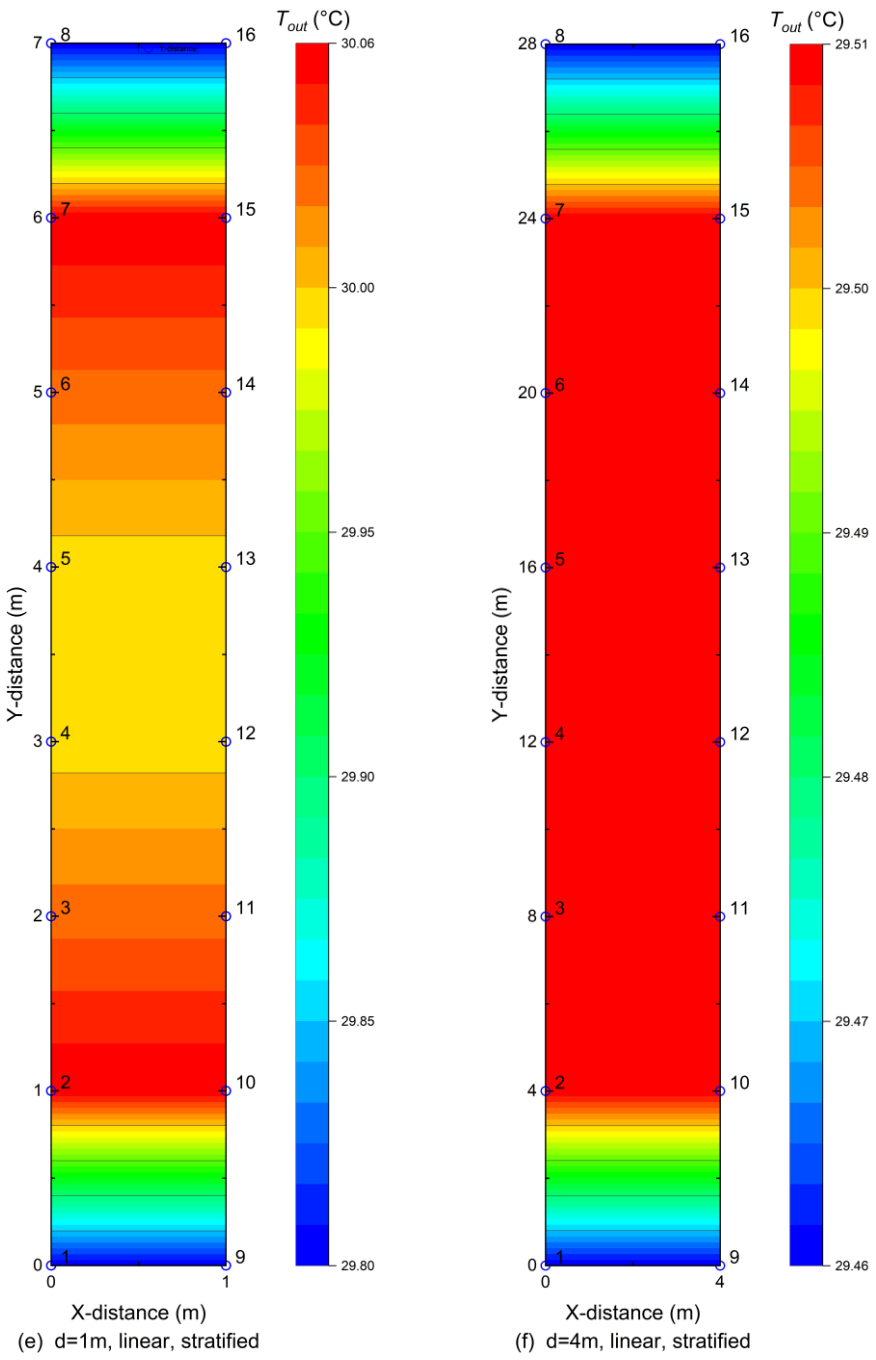

Fig. 10 Outlet fluid temperature (T_{out}) contours for individual boreholes with spacings of 1 m and 4 m in stratified ground: (a)-(b) square, (c)-(d) L-shape, and (e)-(f) linear layout configurations on Day 60

Fig. 11 plots the variations in outlet fluid temperature and heat injection rate for representative boreholes, the most and least affected boreholes as identified in Fig. 10, with a 1-m spacing in stratified ground across three layout configurations. The single borehole scenario is included for comparison. As the outlet fluid temperature gradually increases, the heat injection rate of the boreholes decreases. Due to heat interference among boreholes, the outlet fluid temperatures of individual boreholes in the field

are higher than those in the single borehole scenario, corresponds to a lower heat injection rate. Notably, the outlet temperatures of the most affected boreholes in all three layout configurations would exceed 30 ℃, a negative heat injection rate is obtained, meaning that heat is actually being extracted from these boreholes. Additionally, when comparing the least affected boreholes with the single borehole scenario, the heat injection rates of the least affected boreholes in the square, L-shape, and linear layout configurations on Day 60 are reduced by 53.98%, 55.98%, and 67.06%, respectively, in this analysis.

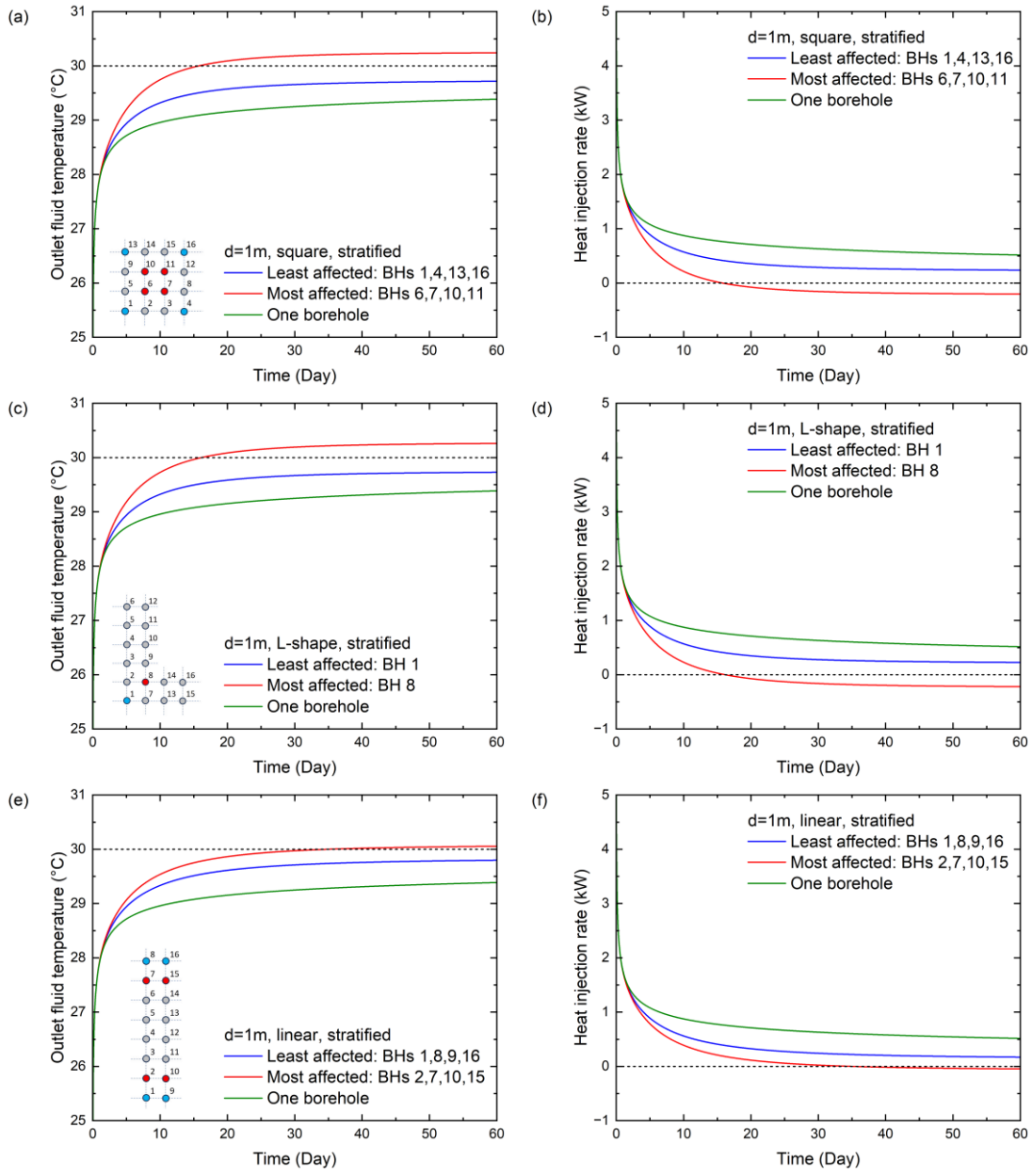

Fig. 11 Outlet fluid temperature and heat injection rates of representative boreholes with a 1-m spacing in stratified ground: (a) square, (b) L-shape, and (c) linear configurations (BH means borehole)

774 The above observations demonstrate that the borehole layout configuration, essentially the inherent
775 thermal interference, significantly influence the outlet fluid temperature distribution and differences
776 among boreholes, further affecting the heat injection rate of individual boreholes. Owing to the thermal
777 interaction within the borehole field, each borehole displays distinct thermal performance compared to
778 the single borehole scenario. However, as the borehole spacing increases to 4 m in this analysis, these
779 effects diminish, resulting in a more uniform outlet fluid temperature distribution within the borehole
780 field.
781
782 **5.2.3 Effects of ground stratification on average outlet fluid temperature and heat injection rate of**
783 **borehole field**
784 Fig. 12(a) compares the average outlet fluid temperatures of the square-layout borehole field in both
785 stratified and homogenous ground conditions across various borehole spacings. The figure shows that
786 the average outlet fluid temperature in stratified conditions consistently surpasses that in homogenous
787 conditions. This disparity is due to ground stratification, where the differing thermophysical properties
788 of the three ground layers lead to varying degrees of thermal interaction among borehole sections in
789 different ground layers (Olfman et al., 2014; Jin et al., 2020). Furthermore, the temporal evolution of the
790 temperature discrepancy between stratified and homogeneous conditions varies with borehole spacing.
791 At shorter spacings (1 m or 2 m in this analysis), the discrepancy declines over time, while at larger
792 spacings (3 m or 4 m in this analysis), it increases. For instance, at a 2-m spacing, the discrepancy reduces
793 from 0.08 ℃ on Day 10 to 0.02 ℃ on Day 60, whereas at a 4-m spacing, it increases from 0.03 ℃ on
794 Day 10 to 0.06 ℃ on Day 60. This behaviour can be attributed to the thermal interference among
795 boreholes, which intensifies as spacing decreases. When boreholes are closely spaced, the discernible
796 impact of thermal interference on average outlet fluid temperature outweighs that attributable to
797 homogeneous ground conditions. Similar trends are observed for borehole fields configured in L-shape
798 or linear layouts. This indicates that for a closely arranged borehole field, treating the ground as
799 homogeneous is acceptable, with minimal influence on the long-term thermal performance of borehole
800 field. However, for a sparsely arranged borehole field, the ground stratification should be considered.
801 Fig. 12(b) presents the heat injection rates of the square-layout borehole field at spacings ranging from
802 1 m to 4 m. The figure indicates that homogenous ground generally yields higher heat injection rates
803 compared to stratified ground in this analysis. For instance, at a 2-m spacing, the heat injection rate is

13.71 kW on Day 10 under homogeneous conditions, whereas it is 12.63 kW under stratified conditions. Moreover, the discrepancy between these two ground conditions increases over time when the spacing is 3 m or more in this analysis. This suggests that assuming homogenous ground would result in lower thermal interactions among boreholes. Consequently, designing a GSHP system in stratified ground using a homogenous ground model with equivalent thermal properties would overestimate the heat injection performance of the borehole field and lead to undersizing of the borehole ground heat exchangers. This finding is consistent with Zhang et al. (2022). The analysis demonstrates the significance of accounting for ground stratification in governing the thermal behaviour of borehole fields, a crucial aspect addressed by the proposed model in this study.

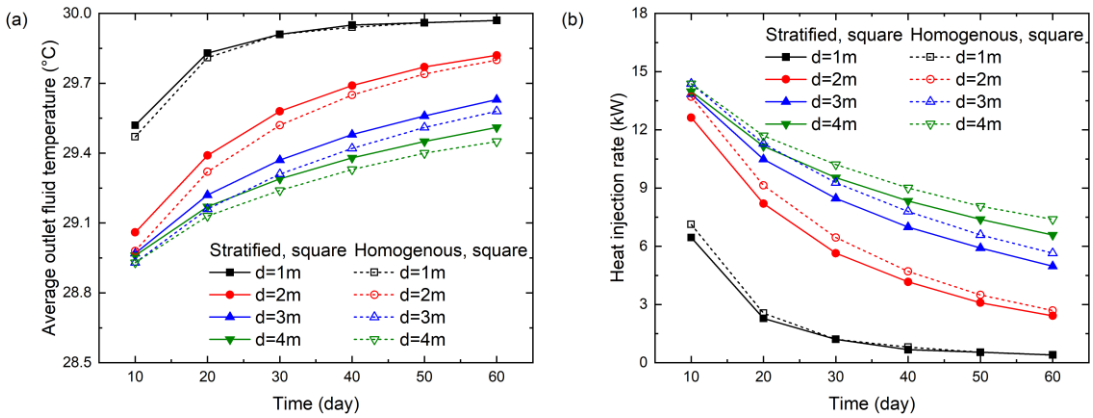

Fig. 12 Effect of ground stratification on (a) average outlet fluid temperature and (b) heat injection rate of borehole field in square layout configuration across various borehole spacings

5.2.4 Effects of ground stratification on fluid temperature and heat injection rate of representative boreholes

Fig. 13(a) and Fig. 13(b) show the outlet fluid temperature contours on Day 60 for indivisible boreholes in a square layout within homogenous ground, with spacings of 1 m and 4 m, respectively. Similar to the stratified ground conditions in Fig. 10(a) and Fig, 10(b), the core boreholes (BHs 6, 7, 10, and 11) have the highest outlet temperatures, while the corner boreholes (BHs 1, 4, 13, and 16) have the lowest. When comparing Fig. 13(a) and Fig. 10(a) at a 1-m spacing, the highest and lowest outlet temperatures are nearly identical, consistent with the negligible discrepancy in the average outlet temperature as shown in Fig. 12(b). In contrast, at a larger spacing of 4 m in this analysis, Fig. 13(b) shows the highest and lowest outlet temperatures in homogenous conditions as 29.48 ℃and 29.43 ℃,

respectively, compared to 29.55 ℃ and 29.46 ℃ in stratified conditions in Fig. 10(b). This difference is reflected in the noticeable variation in the average outlet temperature as shown in Fig. 12(b). The comparison again shows that ground stratification has varying degrees of impact on the thermal performance of the borehole field under different spacing conditions. When borehole spacing is large, which is 4 m in this analysis, ground stratification needs to be considered.

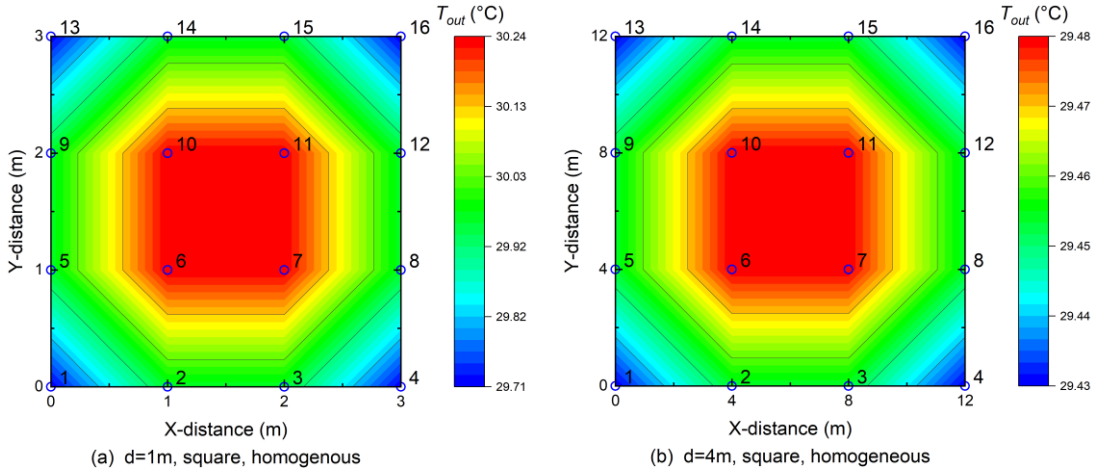

Fig. 13 Outlet fluid temperature (T_{out}) contours for individual boreholes in square layout and homogenous ground with spacings of (a)1 m and (b) 4 m on Day 60

Fig. 14 presents the outlet fluid temperatures and heat injection rates of the most and least affected boreholes in a square layout with 4-m spacing in stratified and homogenous ground. As shown in Fig. 14(a), the difference in outlet fluid temperatures between the most and least affected boreholes increase over time, regardless of ground stratification. However, a greater temperature difference is observed in stratified ground compared to homogenous ground in this analysis. Consequently, as shown in Fig. 14(b), the heat injection rate of the most affected boreholes in stratified conditions is reduced by 17% on Day 60 compared to the least affected ones, while in homogenous conditions, this reduction is 10%. These results indicate that assuming homogenous ground conditions would diminish the thermal performance differences among boreholes.

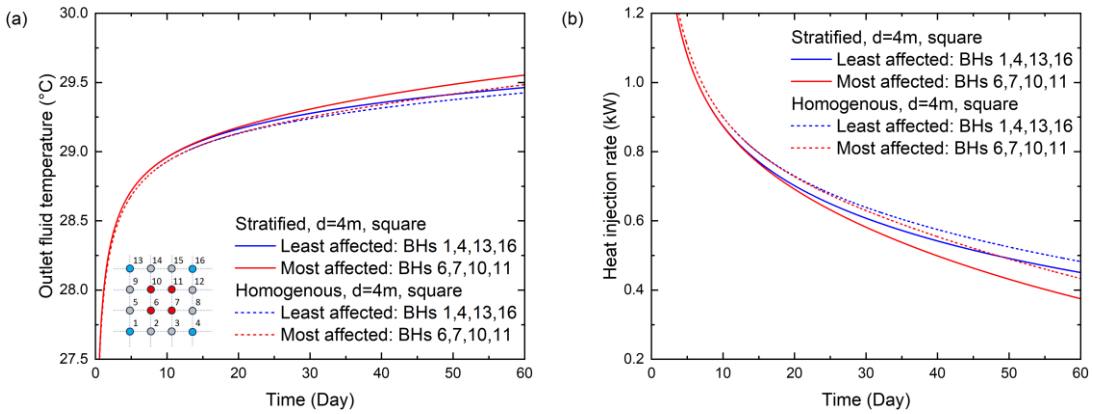

Fig. 14 Results of the representative boreholes in the square layout with 4-m spacing: (a) outlet fluid temperature and (b) heat injection rate (BH means borehole)

In the square layout with 4-m spacing, the least affected borehole (BH 1) and the most affected borehole (BH 6) are selected to compare borehole wall temperatures (e.g., ground temperatures adjacent to boreholes) under stratified and homogenous ground conditions, as shown in Fig. 15. For both boreholes, the temperature distributions in stratified ground conditions differ markedly from those in homogenous conditions due to the varying thermal diffusivity across the three ground layers. In stratified ground, ground layers with lower thermal diffusivity exhibit greater temperature responses compared to those with higher diffusivity, consistent with heat conduction principles. Transition zones are observed at the interfaces between ground layers. In contrast, homogeneous conditions result in a unified temperature response with no transition zones. Since the thermal diffusivity of the homogenous ground (5.99e-7 m^2/s) is similar to that of Layer 3 (5.81e-7 m^2/s) in this analysis, temperatures in Layer 3 are comparable. These findings align with Pan et al. (2020) and Zhang et al. (2022), indicating that the homogeneity assumption can lead to significant deviations in thermal response, potentially overestimating or underestimating temperatures in different layers.

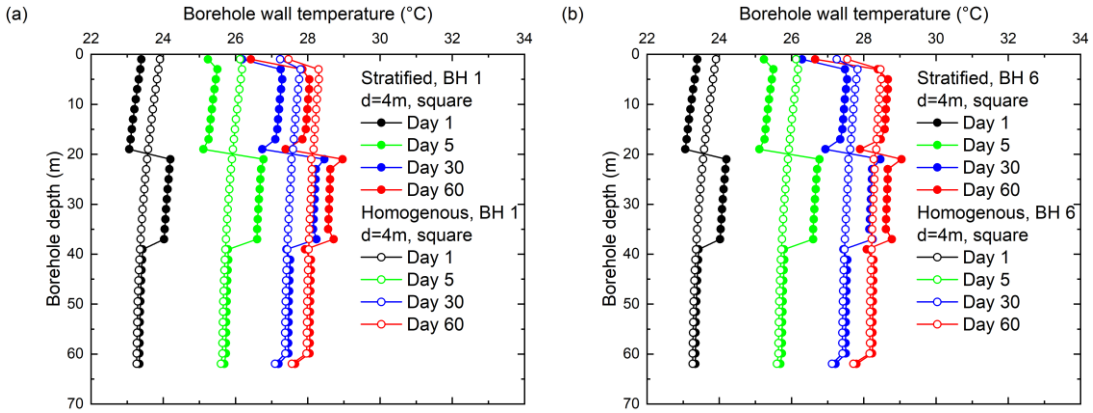

Fig. 15 Borehole wall temperatures of representative boreholes in square layout configuration with a spacing of 4 m: (a) stratified ground and (b) homogenous ground (BH means borehole)

In further analysis of the least affected borehole (BH 1) and the most affected borehole (BH 6) in the square layout with a 4-m spacing, heat flux comparisons along the borehole depth in stratified and homogenous grounds are illustrated in Fig. 16. The heat flux decreases over time due to thermal interference among boreholes, with this effect being more pronounced for the core borehole (BH 6) compared to the corner borehole (BH 1). Stratified ground conditions significantly alter the heat flux across the three ground layers, while the heat flux remains nearly uniform in homogenous ground, consistent with the findings by Zhang et al. (2022). This comparison highlights the importance of ground stratification in influencing borehole eat flux, which has implications for the proper sizing of borehole ground heat exchangers.

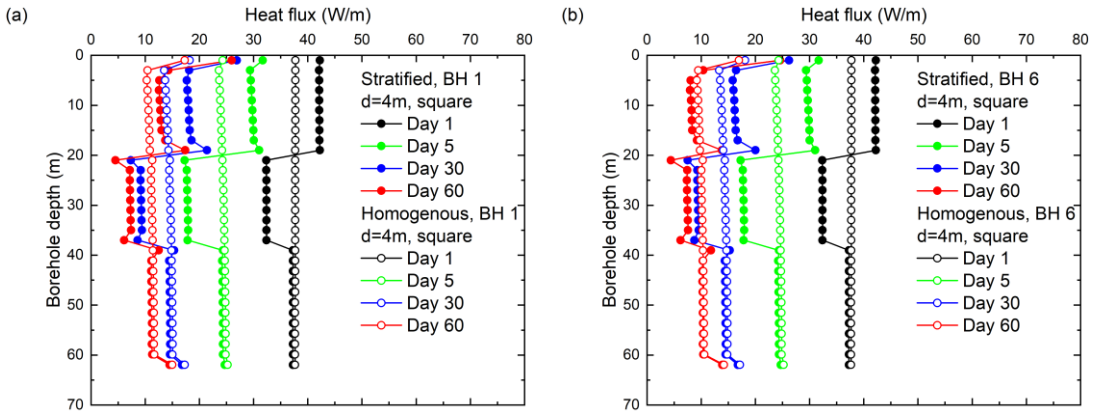

Fig. 16 Comparison of heat flux along the borehole depth in stratified and homogenous grounds: (1) BH 1 and (2) BH 6 in square layout configuration with a spacing of 4 m (BH means borehole)

The above observations demonstrate that ground stratification significantly influences both fluid and ground temperatures, further affecting the heat injection rate and the sizing of boreholes. Assuming homogeneous ground conditions would reduce the variations in thermal performance among boreholes. Ground stratification should be considered when estimating the thermal performance of a borehole field, particularly when the boreholes are sparsely arranged (e.g., with spacing of 3 m or more, as examined in this analysis).

6. Discussion

As reviewed in the previous sections, simulating borehole ground heat exchangers in stratified ground presents considerable complexity but holds significant engineering value. Table 3 summarizes the existing analytical models in the literature and compares their features.

Al-Khoury and Focaccia (2016) proposed a semi-analytical model based on spectral analysis to simulate heat flow in an axisymmetric shallow geothermal system, specifically for a double U-tube borehole in homogenous ground. Later, BniLam and Al-Khoury (2017) introduced a spectral element formulation for nonhomogeneous heat flow, assuming uniform heat flux along the borehole depth. However, this spectral element method does not offer an explicit solution for stratified ground conditions. Pan et al. (2020) employed an integral-transform method based on the Laplace transform for boreholes in layered ground, but this model cannot accommodate multiple boreholes or the heat transfer inside each borehole.

The development of thermal network models is a widely adopted approach for analyzing heat transfer within boreholes. For instance, Belzile et al. (2016a) combined a thermal network model with a control-volume finite difference method to model the borehole field, although their model does not account for stratified ground. Morchio and Fossa (2021) utilized a thermal network model alongside the full Fourier equation for layered ground, but their model has not been expanded to scenarios involving multiple boreholes. Meanwhile, Alaie et al. (2021) and Guo et al. (2023) developed composite analytical models based on the finite source model and thermal network model. However, these models either do not apply to layered ground conditions or multiple boreholes.

The segmented FLS model and composite section concept proposed by Abdelaziz et al. (2014) are commonly used to simulate heat transfer outside borehole in stratified ground. Models developed by Hu (2017), Erol and François (2018), Jin et al. (2020), and Luo et al. (2021) follow this approach, where the

914 temperature response at a specific point in layered ground is obtained by summing up the contributions
915 of all borehole segments, with composite thermal properties used to predict the thermal response of
916 segments located outside the segmental source layer. This approach allows for the consideration of
917 stratified ground conditions. However, these models each have limitations, including the inability to
918 account for nonuniform heat flux along the borehole depth or unsuitability for multiple boreholes.

919 Additionally, Zhang et al. (2022) first developed an analytical model using Green's function method
920 to describe the thermal response outside boreholes in layered ground. This model conceptualizes the
921 borehole's cylindrical surface as a series of stacked ring coils, employing Green's function theory to
922 capture the heat transfer dynamics. A numerical model was further established to investigate the thermal
923 behaviour of the circulating fluid and grouting material inside the boreholes.

924 The proposed composite analytical model in this study offers distinct advantages and characteristics
925 compared to other models in the literature. By dividing the borehole field into two regions, this model,
926 as a whole, characterizes transient heat transfer both within and outside the borehole using a simplified
927 thermal network model and a segmented finite line source model that accommodates variable heat flux
928 along the borehole depth. The borehole wall temperature serves as a crucial link, allowing thermal
929 interactions among boreholes to influence the internal heat transfer of boreholes. Additionally, by
930 discretizing the ground into sections and accounting for the different thermophysical properties of each
931 ground layer, the proposed model effectively incorporates the effects of ground stratification.
932 Consequently, this composite analytical model is highly effective for assessing the thermal performance
933 of multiple boreholes in multilayered ground conditions.
934

935 Table 3 Comparison of developed analytical models

Model	Model features, including methods used in the solution to the ground response	Stratified ground	Ground water flow	Multiple boreholes	Nonuniformity of heat flux along depth	Model inside the borehole	Model outside the borehole	Configuration of pipes
Abdelaziz et al. (2014)	Segmented finite line source model with composite section concept	√	×	×	√	×	√	Single U-tube
Al-Khoury and Focaccia (2016)	Spectral analysis method	×	×	×	×	√	√	Double U-tube
Belzile et al. (2016a)	Control-volume finite difference method and thermal network model	×	×	√	√	√	√	Single U-tube
BniLam and Al-Khoury (2017)	Spectral element method	√	×	×	×	√	√	Single U-tube
Hu (2017)	Moving finite source model and thermal network model	√	√	×	×	√	√	Single U-tube
Erol and François (2018)	Moving finite source model and composite section concept	√	√	×	×	×	√	NA
Jin et al. (2020)	Segmented finite line source and composite section concept	√	×	√	×	×	√	NA
Pan et al. (2020)	Integral-transform method	√	×	×	√	×	√	NA
Morchio and Fossa (2021)	Finite difference scheme of the Fourier equation and thermal network model	√	×	×	√	√	√	Single or double U-tube
Alaie et al. (2021)	Finite line source model and thermal network model	×	×	√	√	√	√	Single U-tube
Luo et al. (2021)	Segmented finite line source model with composite section concept	√	×	×	√	√	√	Coaxial
Zhang et al. (2022)	Separation of variables and Green's function method and numerical model	√	×	√	√	√	√	Single U-tube
Guo et al. (2023)	Fine line source model with Green's function method and thermal network model	√	×	×	√	√	√	Single U-tube
This study	Segmented finite source model with composite section concept, and thermal network model	√	×	√	√	√	√	Single U-tube

936 Note: NA means not available.

937

In addition to the factors considered in the proposed model, the thermal performance of borehole ground heat exchangers is influenced by several other important factors. Groundwater flow, often presents in the subsurface, significantly impacts heat transfer, as it occurs not only through conduction but also via advection due to groundwater movement (Molina-Giraldo et al., 2011; Liuzzo-Scorpo et al., 2015; Hu, 2017; Erol and François, 2018; Cai et al., 2020; Bao et al., 2023). Various configurations of U-tube, including double or multiple designs, have been proposed to enhance the heat exchange efficiency between the boreholes and the surrounding ground (Eslami-nejad and Bernier, 2011; Bauer et al., 2011; Belzile et al., 2016b; Cimmino, 2016). Boreholes usually have a certain buried depth in practice (Cimmino, 2018; Alaie et al., 2021), and heat can transfer vertically through the grouting material in a thermal conductive manner. Moreover, as geothermal energy exploitation extends to greater depths, the natural geothermal gradient of the ground play a significant role in the efficiency of heat extraction and injection of boreholes (Bandos et al., 2009; Luo et al., 2019; Wang et al., 2021). Ongoing efforts are focused on refining the presented model to incorporate these influential factors, thereby aligning it more closely with the real-world situation and broadening its application.

7. Conclusions

In this paper, a new composite analytical model tailored to evaluate the thermal performance of multiple boreholes within layered ground is established. The model integrates critical factors influencing heat transfer, encompassing ground stratification, thermal interactions among boreholes, variability of heat flux along borehole depth, and flexible layouts of boreholes. Combining heat transfer simulations inside and outside the boreholes, thermal data pertinent to borehole fields in stratified ground during heat exchange operations can be obtained efficiently. Implemented in the platform of TRNSYS software, the model offers versatile applicability to GSHP systems, borehole thermal energy storage, and district heating and cooling networks. Model validations through four distinct experiments, covering varied borehole quantities and ground conditions, are carried out. Using this model, the thermal performance of a borehole field comprising 16 boreholes with spacing from 1 m to 4 m in a three-layer ground is investigated over a 60-day period of warm water injection at 30 °C. The effects of borehole layout and ground stratification on the thermal performance of individual and collective boreholes are analysed. The key conclusions from this analysis are as follows:

(1) The proposed composite analytical model is capable of capturing the measured temperature

evolution in outlet fluid for the four cases, with the RSME between the model predictions and measurements ranged from 0.27 ℃ to 0.69 ℃, the MAE ranged from 0.17 ℃ to 0.50 ℃, and the MAPE ranged from 0.75% to 2.02%, showing good agreement with the measured data.

(2) Borehole layout configuration, essentially the inherent thermal interference, significantly influences the outlet fluid temperature distribution and differences among boreholes, further affecting the heat injection rate of individual boreholes. Across the square, L-shape, and linear layout configurations, the impact of layout on the thermal performance of borehole fields diminishes when the borehole spacing reaches 4 m in this analysis.

(3) The positions of the most and least affected boreholes by thermal interferences vary by layout. In the square layout, core boreholes are most affected, while corner boreholes are least affected. In the L-shape layout, boreholes at the inner corners experience the most thermal interference, and those at the outer corners the least. In the linear layout, boreholes in the second-row inward along the x-direction are most affected, while those in the outermost rows are least affected in this analysis.

(4) Compared to a single borehole scenario, significant heat interference among boreholes leads to increased outlet fluid temperature and reduced thermal injection rate, with this trend amplifying with decreasing borehole spacing. In comparison to the single borehole scenario, at a 1-m spacing, the heat injection rates of the least affected boreholes in square, L-shape, and linear layouts are reduced by 53.98%, 55.98%, and 67.06%, respectively, by Day 60 in this analysis.

(5) Ground stratification significantly influences fluid and ground temperatures, thereby affecting heat injection rate and borehole sizing. The average outlet fluid temperature in stratified ground consistently exceeds that in homogenous ground, resulting in a lower heat injection rate. Designing a GSHP system in stratified ground using a homogenous ground model with equivalent thermal properties would overestimate the heat injection performance of the borehole field and lead to undersizing of the borehole ground heat exchangers.

(6) Assuming homogenous ground conditions would diminish the thermal performance differences among boreholes. In a square layout with a 4-m spacing, the heat injection rate of the most affected boreholes in stratified conditions is reduced by 17% on Day 60 compared to the least affected ones, whereas in homogenous conditions, this reduction is 10%. Ground stratification should be considered when estimating the thermal performance of a borehole field, particularly when the

boreholes are sparsely arranged, e.g., with spacing of 3 m or more, as examined in this analysis.

Acknowledgements

This work was supported by the EPSRC funded "Integrated Heating and Cooling Networks with Heat-sharing-enabled Smart Prosumers" project (Grant number EP/T022795/1). The financial support for the authors is gratefully acknowledged.

References

Abdelaziz, S.L., Ozudogru, T.Y., Olgun, C.G., Martin II, J.R., 2014. Multilayer finite line source model for vertical heat exchangers. Geothermics, 51, 406-416.

Alaie, O., Maddahian, R., Heidarinejad, G., 2021. Investigation of thermal interaction between shallow boreholes in a GSHE using the FLS-STRCM model. Renewable Energy, 175, 1137-1150.

Al-Khoury, R., Focaccia, S., 2016. A spectral model for transient heat flow in a double U-tube geothermal heat pump system. Renewable Energy, 85, 195-205.

Bandeira Neto, L.A., Narsilio, G.A., Makasis, N., 2023. Analytical interpretation and numerical analysis of multiple energy pile thermal response tests. Computers and Geotechnics, 157, 105314.

Bandos, T.V., Montero, Á., Fernández, E., Santander, J.L.G., Isidro, J.M., et al., 2009. Finite line-source model for borehole heat exchangers: effect of vertical temperature variations. Geothermics, 38(2), 263-270.

Bao, L.L., Wang, X., Jin, P.J., Cui, J.Y., Zhu, Y.L., Wang, Y.S., 2023. An analytical heat transfer model for the mid-deep U-shaped borehole heat exchanger considering groundwater seepage. Journal of Building Engineering, 64, 105612.

Bauer, D., Heidemann, W., Müller-Steinhagen, H., Diersch, H.J., 2011. Thermal resistance and capacity models for borehole heat exchangers. International Journal of Energy Research, 35(4), 312-320.

Beier, R.A., Smith, M.D., Spitler, J.D., 2011. Reference data sets for vertical borehole ground heat exchanger models and thermal response test analysis. Geothermics, 40(1), 79-85.

Belzile, P., Lamarche, L., Rousse, D.R., 2016a. Semi-analytical model for geothermal borefields with independent inlet conditions. Geothermics, 60, 144-155.

Belzile, P., Lamarche, L., Rousse, D.R., 2016b. Geothermal heat exchange in boreholes with independent sources. Applied Thermal Engineering, 98, 1221-1230.

Bennet, J., Claesson, J., Hellström, G., 1987. Multipole method to compute the conductive heat flows to and between pipes in a composite cylinder. Notes on Heat Transfer 3-1987. Department of Building Physics, Lund Institute of Technology, Lund, Sweden.

BniLam, N., Al-Khoury, R., 2017. A spectral element model for nonhomogeneous heat flow in shallow geothermal systems. International Journal of Heat and Mass Transfer, 104, 703-717.

Cai, S.S., Li, X.Y., Zhang, M.H., Fallon, J., Li, K., Cui, T.F., 2020. An analytical full-scale model to predict thermal response in boreholes with groundwater advection. Applied Thermal Engineering, 168, 114828.

Cassina, L., Laloui, L., Loria, A.F.R., 2022. Thermal interactions among vertical geothermal borehole fields. Renewable Energy, 194, 1204-1220.

Carslaw, H.S., Jaeger, J.C., 1959. Conduction of heat in solids, 2nd edition, Oxford University Presse, London.

Chen, F., Mao, J., Chen, S., Li, C., Hou, P., Liao, L., 2018. Efficiency analysis of utilizing phase change materials as grout for a vertical U-shape heat exchanger coupled ground source heat pump system. Applied Thermal Engineering, 130, 698-709.

Chen, F., Mao, J., Zhu, G., Zhang, B., Tian, Y., Liao, D., Liu, Y., 2021. Numerical assessment on the thermal imbalance of multiple ground heat exchangers connected in parallel. Geothermics, 96, 102191.

Cimmino, M., 2016. Fluid and borehole wall temperature profiles in vertical geothermal boreholes with multiple U-tubes. Renewable Energy, 96, 137-147.

Cimmino, M., 2018. Fast calculation of the g-functions of geothermal borehole fields using similarities in the evaluation of the finite line source solution. Journal of Building Performance Simulation, 11(6), 655-668.

Erol, S., François, B., 2018. Multilayer analytical model for vertical ground heat exchanger with groundwater flow. Geothermics, 71, 294-305.

Eslami-Nejad, P., Bernier, M., 2011. Coupling of geothermal heat pumps with thermal solar collectors using double U-tube boreholes with two independent circuits. Applied Thermal Engineering, 31(14-15), 3066-3077.

Gao, W., Qadrdan, M., Chaudry, M., Wu, J.Z., 2023a. Seasonal storage of heat in boreholes. Technical note. UK Energy Research Centre.

Gao, W., Masum, S., Jiang, L.L., 2023b. Technical performance comparison of horizontal and vertical

ground-source heat pump systems. Journal of GeoEnergy, 2023(1), 6106360.

Gawecka, K.A., Taborda, D.M., Potts, D.M., Sailer, E., Cui, W., Zdravković, L., 2020. Finite-element modeling of heat transfer in ground source energy systems with heat exchanger pipes. International Journal of Geomechanics, 20(5), 04020041.

Gultekin, A., Aydin, M., Sisman, A., 2019. Effects of arrangement geometry and number of boreholes on thermal interaction coefficient of multi-borehole heat exchangers. Applied energy, 237, 163-170.

Guo, Y., Huang, G., Liu, W.V., 2023. A new semi-analytical solution addressing varying heat transfer rates for U-shaped vertical borehole heat exchangers in multilayered ground. Energy, 274, 127373.

Hefni, M.A., Xu, M.H., Zueter, A.F., Hassani, F., et al., 2022. A 3D space-marching analytical model for geothermal borehole systems with multiple heat exchangers. Applied Thermal Engineering, 216, 119027.

Hu, J., 2017. An improved analytical model for vertical borehole ground heat exchanger with multiple-layer substrates and groundwater flow. Applied Energy, 202, 537-549.

Ingersoll L.R., 1954. Heat conduction: with engineering, geological, and other applications. University of Wisconsin Press.

Ingersoll L.R., Plass H.J., 1948. Theory of the ground pipe source for the heat pump. ASHRAE Transactions. 54, 339-48.

Jin, G., Li, Z., Guo, S.P., Wu, X., Wu, W.F., Zhang, K., 2020. Thermal performance analysis of multiple borehole heat exchangers in multilayer geotechnical media. Energy, 209, 118236.

Koohi-Fayegh, S., Rosen, M.A., 2012. On thermally interacting multiple boreholes with variable heating strength: Comparison between analytical and numerical approaches. Sustainability, 4(8), 1848-1866.

Kurevija, T., Vulin, D., Krapec, V., 2012. Effect of borehole array geometry and thermal interferences on geothermal heat pump system. Energy Conversion and Management, 60, 134-142.

Kurnia, J.C., Putra, Z.A., Muraza, O., Ghoreishi-Madiseh, S.A., Sasmito, A.P., 2021. Numerical evaluation, process design and techno-economic analysis of geothermal energy extraction from abandoned oil wells in Malaysia. Renewable Energy, 175, 868-879.

Lamarche, L., Beauchamp, B., 2007a. A new contribution to the finite line-source model for geothermal boreholes. Energy and Buildings, 39(2), 188-198.

Lamarche, L., Beauchamp, B., 2007b. New solutions for the short-time analysis of geothermal vertical

boreholes. International Journal of Heat and Mass Transfer, 50(7-8), 1408-1419.

Lamarche, L., Kajl, S., Beauchamp, B., 2010. A review of methods to evaluate borehole thermal resistances in geothermal heat-pump systems. Geothermics, 39(2), 187-200.

Law, Y.L.E., Dworkin, S.B., 2016. Characterization of the effects of borehole configuration and interference with long term ground temperature modelling of ground source heat pumps. Applied Energy, 179, 1032-1047.

Lax, P., Wendroff, B., 1960. Systems of conservation laws. Communications on Pure and Applied Mathematics, 13(2), 217–237.

Lee, C.K., 2011. Effects of multiple ground layers on thermal response test analysis and ground-source heat pump simulation. Applied Energy, 88(12), 4405-4410.

Lee, C.K., Lam, H.N., 2008. Computer simulation of borehole ground heat exchangers for geothermal heat pump systems. Renewable Energy, 33(6), 1286-1296.

Lee, C.K., Lam, H.N., 2012. A modified multi-ground-layer model for borehole ground heat exchangers with an inhomogeneous groundwater flow. Energy, 47(1), 378-387.

Li, M., Lai, A.C., 2012. Heat-source solutions to heat conduction in anisotropic media with application to pile and borehole ground heat exchangers. Applied Energy, 96, 451-458.

Li, W.F., Hu, Z.C., Geng, S.W., Wang, F.Y., Liu, X.Y., Guo, Y.B., Huang, H., Han, Y.C., 2023. Study on the influence of borehole heat exchanger structure and soil thermal property on soil heat storage characteristics of the HST-BHE system. Applied Thermal Engineering, 231, 120915.

Li, W.X., Li, X.D., Du, R.Q., Wang, Y., Tu, J.Y., 2019. Experimental investigations of the heat load effect on heat transfer of ground heat exchangers in a layered subsurface. Geothermics, 77, 75-82.

Li, W.X., Li, X.D., Peng, Y.L., Wang, Y., Tu, J.Y., 2018. Experimental and numerical investigations on heat transfer in stratified subsurface materials. Applied Thermal Engineering, 135, 228-237.

Li, W.X., Li, X.D., Peng, Y.L., Wang, Y., Tu, J.Y., 2020. Experimental and numerical studies on the thermal performance of ground heat exchangers in a layered subsurface with groundwater. Renewable Energy, 147, 620-629.

Liuzzo-Scorpo, A., Nordell, B., Gehlin, S., 2015. Influence of regional groundwater flow on ground temperature around heat extraction boreholes. Geothermics, 56, 119-127.

Luo, Y.Q., Guo, H.S., Meggers, F., Zhang, L., 2019. Deep coaxial borehole heat exchanger: Analytical modeling and thermal analysis. Energy, 185, 1298-1313.

Marcotte, D., Pasquier, P., 2009. The effect of borehole inclination on fluid and ground temperature for GLHE systems. Geothermics, 38(4), 392-398.

Miglani, S., Orehounig, K., Carmeliet, J., 2018. A methodology to calculate long-term shallow geothermal energy potential for an urban neighbourhood. Energy and Buildings, 159, 462-473.

Minaei, A., Maerefat, M., 2017a. Thermal resistance capacity model for short-term borehole heat exchanger simulation with non-stiff ordinary differential equations. Geothermics, 70, 260-270.

Minaei, A., Maerefat, M., 2017b. A new analytical model for short-term borehole heat exchanger based on thermal resistance capacity model. Energy and Buildings, 146, 233-242.

Molina-Giraldo, N., Blum, P., Zhu, K., Bayer, P., Fang, Z., 2011. A moving finite line source model to simulate borehole heat exchangers with groundwater advection. International Journal of Thermal Sciences, 50(12), 2506-2513.

Morchio, S., Fossa, M., 2021. Modelling and validation of a new hybrid scheme for predicting the performance of U-pipe borehole heat exchangers during distributed thermal response test experiments. Applied Thermal Engineering, 186, 116514.

Olfman, M.Z., Woodbury, A.D., Bartley, J., 2014. Effects of depth and material property variations on the ground temperature response to heating by a deep vertical ground heat exchanger in purely conductive media. Geothermics, 51, 9-30.

Pan, A., McCartney, J.S., Lu, L., You, T., 2020. A novel analytical multilayer cylindrical heat source model for vertical ground heat exchangers installed in layered ground. Energy, 200, 117545.

Pasquier, P., Marcotte, D., 2012. Short-term simulation of ground heat exchanger with an improved TRCM. Renewable Energy, 46, 92-99.

Pokhrel, S., Sasmito, A.P., Sainoki, A., Tosha, T., Tanaka, T., Nagai, C., Ghoreishi-Madiseh, S.A., 2022. Field-scale experimental and numerical analysis of a downhole coaxial heat exchanger for geothermal energy production. Renewable Energy, 182, 521-535.

Ricks, W., Voller, K., Galban, G., Norbeck, J.H., Jenkins, J. D., 2024. The role of flexible geothermal power in decarbonized electricity systems. Nature Energy, 1-13.

Ruiz-Calvo, F., De Rosa, M., Acuña, J., Corberán, J.M., Montagud, C., 2015. Experimental validation of a short-term Borehole-to-Ground (B2G) dynamic model. Applied Energy, 140, 210-223.

Ruiz-Calvo, F., De Rosa, M., Monzó, P., Montagud, C., Corberán, J.M., 2016. Coupling short-term (B2G model) and long-term (g-function) models for ground source heat exchanger simulation in

TRNSYS. Application in a real installation. Applied Thermal Engineering, 102, 720-732.

Shen, J.H., Zhou, C.H., Luo, Y.Q., Tian, Z.Y., Zhang, S.C., Fan, J.H., Ling, Z., 2023. Comprehensive thermal performance analysis and optimization study on U-type deep borehole ground source heat pump systems based on a new analytical model. Energy, 274, 127367.

Sutton, M.G., Couvillion, R.J., Nutter, D.W., Davis, R.K., 2002. An algorithm for approximating the performance of vertical bore heat exchangers installed in a stratified geological regime. ASHRAE Transactions, 108, 177.

The Engineering ToolBox, 2024. https://www.engineeringtoolbox.com.

TRNSYS Simulation Studio, 2023. Version 18.0, The University of Wisconsin, Madison, US.

Wang, C.L., Lu, Y.H., Chen, L.W., Huang, Z.J., Fang, H., 2021. A semi-analytical model for heat transfer in coaxial borehole heat exchangers. Geothermics, 89, 101952.

Yang, W.B., Shi, M.H., Liu, G.Y., Chen, Z.Q., 2009. A two-region simulation model of vertical U-tube ground heat exchanger and its experimental verification. Applied Energy, 86(10), 2005-2012.

Yang, W.B., Zhang, S.S., Chen, Y.P., 2014. A dynamic simulation method of ground coupled heat pump system based on borehole heat exchange effectiveness. Energy and Buildings, 77, 17-27.

Zarrella, A., Scarpa, M., De Carli, M., 2011. Short time step analysis of vertical ground-coupled heat exchangers: The approach of CaRM. Renewable Energy, 36(9), 2357-2367.

Zeng, H.Y., Diao, N.R., Fang, Z.H., 2002. A finite line-source model for boreholes in geothermal heat exchangers. Heat Transfer—Asian Research: Co-sponsored by the Society of Chemical Engineers of Japan and the Heat Transfer Division of ASME, 31(7), 558-567.

Zhang, D.H., Zhao, P., Li, X.Z., Zhou, Y., Gao, P.H., Zhang, Y., Zhang, C.Y., 2022. Heat transfer analysis of a borehole heat exchanger array in a layered subsurface. Applied Thermal Engineering, 216, 119076.

Zhou, Y., Wu, Z.H., Wang, K., 2021. An analytical model for heat transfer outside a single borehole heat exchanger considering convection at ground surface and advection of vertical water flow. Renewable Energy, 172, 1046-1062.

Zong, Y., Valocchi, A.J., Lin, Y.F.F., 2023. Coupling a borehole thermal model and MT3DMS to simulate dynamic ground source heat pump efficiency. Groundwater, 61(2), 237-244.